2-2014

An experimental investigation into the mechanisms of bacterial evolution

Zhenmao Wan
Graduate Center, City University of New York

An experimental investigation into the mechanisms of bacterial evolution

BY

Zhenmao Wan

A dissertation submitted to the Graduate Faculty in Physics

in partial fulfillment of the requirements for the degree of Doctor of Philosophy

The City University of New York

2014

This manuscript has been read and accepted for the
Gradudate Faculty in Physics in satisfaction of the
dissertation requirement for the degree of Doctor of Philosophy

---

Mark Hillery
Chair of the Examining Committee

Date

Steve Greenbaum
Executive Officer

Date

Supervisory Committee:

William Bialek

Daniel Dykhuizen

Noel Goddard

Neepa Maitra

Weigang Qiu

The City University of New York

An experimental investigation into the mechanisms of bacterial evolution

by

Zhenmao Wan

Adviser: Noel Goddard

Abstract

This thesis studies the two fundamental mechanisms of bacterial evolution — horizontal gene transfer and spontaneous mutation, in the bacterium *Escherichia coli* through novel experimental assays and mathematical simulations. First, I will develop a growth assay utilizing the quantitative polymerase chain reaction (qPCR) to provide real-time enumeration of genetic marker abundance within bacterial populations. Second, I will focus on horizontal gene transfer in *E. coli* occurring through a process called conjugation. By fitting the qPCR data to a resource limited, logistic growth model, I will obtain estimated values of several key parameters governing the dynamics of DNA transfer through conjugation under two different conditions: i) in the absence of selection; ii) in the presence of negative selection pressure — bacteriophage infection. Last, I will investigate spontaneous mutation through qPCR assay of competition between wild-type and mutator phenotype *E. coli*. Mutator phenotype has an elevated mutation rate due to defects in DNA proofreading and repairing system. By introducing antibiotic selective pressure, I will examine the fixation probability of mutators competing with wild-type in novel environment. I also will utilize simulations to study the impact of three parameters on the fixation probability.

Acknowledgments

This thesis would not exist without many people who helped me along the five-and-half-year long journey.

I would like to thank first is my dear mentor Dr. Noel Goddard. It was her trust and patience five years ago that brought me into this fascinating field that bridges biology and physics. It was also her encouragement and motivation that kept me going even after countless failed experiments. My deepest gratitude goes to you, Dr. Noel Goddard, for being the best mentor and friend.

I would like to thank all my committee members and I feel extremely gratefully to have the opportunity to work with all of you: Dr. Weigang Qiu for kindly supporting me financially and patiently guiding my research during the past semester; Dr. William Bialek for sharing your immense repertoire of knowledge through your intellectually stimulating lectures and notes; Dr. Mark Hillery, Dr. Neepa Maitra, and Dr. Daniel Dykhuizen for your insightful comments and valuable advices.

I am also thankful to all the colleagues and friends who supported, helped and inspired me: Physics department: Dr. Marilyn Rothschild, Yin Cen, Jorge Colon, Bo Gao, Yu Gong, Kay Hiranaka, Tetiana Nosach, Georgina Olivares-Renteria, Andi Shehu, Vadim Yerokhin. Goddard lab members: Amal El bakhar, Dima Gorenshteyn, Syed Hasan, Fabiola Louis, Alexsandr Nosonovs, Frances-Camille Padlan, Mariola

Szenk, Sushma Teegala, Joseph Varshavsky, Meisze Yau. CUNY friends: Daniel Byrnes, Xiaoze Liu, Jia Ma, Cheng Peng, Jeff Secor, Chonlong Yu, Xiankan Zhang, Shu Zhao, Xin Zhao.

Finally, many thanks to my parents and all the people whose name did not get acknowledged above for accompanied me through this rewarding journey to become a doctor.

Contents

Listing of tables

Listing of figures

1

Introduction

In 1928, Alexander Fleming, Professor of Bacteriology at St. Mary's Hospital in London, came back from holiday and was sorting through his petri dishes containing bacterium *Staphylococcus*. He noticed mold was growing on one culture plate, which was not too unusual. But what surprised him was the area immediately around the mold was clear, as if something secreted by the mold had killed the bacteria. Later the mold was identified as a rare strain of *Penicillium notatum*, and the bacteria killing compound penicillin became the first identified antibiotic [1]. From then on, more and more antibiotics were discovered along the way that greatly reduced the number of deaths resulting from bacterial infections. However,

this human scientific triumph has been shadowed by nature's counterforce — antibiotic resistance. The U.S. Centers for Disease Control and Prevention (CDC) states in its Antibiotic Resistance Threats in the United States, 2013 Report [2]:

> Antimicrobial resistance is one of our most serious health threats … Each year in the United States, at least 2 million people acquire serious infections with bacteria that are resistant to one or more of the antibiotics designed to treat those infections. At least 23,000 people die each year as a direct result of these antibiotic-resistant infections. Many more die from other conditions that were complicated by an antibiotic resistant infection.

Bacteria can acquire antibiotic resistance in two ways: i) internally by self spontaneous genetic mutation; ii) externally by acquiring an antibiotic resistant gene from another bacterium. These two processes correspond to the two primary fundamental mechanisms of bacterial genome evolution (via genomic plasticity): i) spontaneous mutation of the microbes' genome through external damage (e.g. chemical, radioactive) or internal errors (e.g. faulty replication or repair mechanisms), or ii) obtaining novel genes externally through horizontal gene transfer (HGT). Both mechanisms yield genetic novelty which, in turn, can enable novel phenotypic functionality that may increase microbes' fitness.

Bacterial genome evolution has posed an increasing challenge for us due to its implications in pathogenicity [3, 4] and acquired antibiotic resistance [5, 6]. To provide a more thorough insight, this thesis presents the development of novel experimental assays and mathematical models to quantify the physical parameters and examine their effects associated with these two fundamental mechanisms of bacterial evolution.

1.1 Evolution in the Microbial World

The theory of evolution by means of natural selection describes the process of progeny with higher fitness becoming more common over generations, whereas the ones with lower fitness become less common. The

term “fitness”, in the language of population and evolutionary sense, describes the effectiveness of organisms to utilize resources in the environment to survive and reproduce [7]. Optimizing either survival or reproduction increases organisms’ opportunity to saturate the environment with individuals from their own genetic background. Genetic novelty provides the raw material for this optimization process, and when subjected to selective pressure, it then becomes the driving force for adaptation. Genetic novelty is only useful to an organism’s fitness if the genes are both i) expressed by the organism (vs. junk DNA) and ii) beneficial to the surviving under the selective condition.

Though a large body of theory addresses the kinetic and dynamic process leading to adaptation under selection, laboratory testing of these theories in a controlled environment is only made practical through the study of microbial populations. Due to their small size and short generation time, bacteria allow population studies on the laboratory scale (reviewed in [8, 9]).

Historically, the first intentional cultivation of microbial populations by humans (other than our personal microbiomes) was probably fermentation. Quantitative work began in the mid-20th century, pioneered by French biologist Jacques Monod [10] in batch cultures, and later extended to continuous cultures in chemostats by Aaron Novick and Leó Szilárd [11] (after these two former Manhattan Project physicists switched field from nuclear reactors to bio-reactors). Fermentors and bio-reactors are now commercially available on the pilot (and industrial) scale and continue to increase in technological sophistication. These platforms as well as repeated batch serial dilution techniques [12] have enabled growth and adaptation experiments over 10^2 to 10^5 generations, allowing researchers to begin to quantify and model the driving forces of bacterial evolution.

1.2 Horizontal Gene Transfer

In 1928, British bacteriologist Frederick Griffith conducted the first widely accepted experiments that started the scientific pursuit to understand horizontal gene transfer (HGT). Griffith demonstrated that avirulent

bacterium *Streptococcus pneumoniae* type III-S (smooth) strain can transform into virulent type II-R (rough) strain when the smooth strain is injected into mice together with heat-killed rough strain [13]. The nature of Griffith's transforming principle was finally decoded by one of the founding fathers of modern genetics — Oswald Avery. In 1944, Avery, leading the Rockefeller University team that includes Maclyn McCarty and Colin Macleod, identified the pneumonia inducing gene transfered from the rough strain to the smooth strain was carried by DNA, thus proved the carrier of genes is DNA instead of the prevailing believed protein [14]. Transformation — bacterial cells taking up exogenous DNA from surrounding environment through cell membrane, is the first identified mechanisms of HGT.

Joshua Lederberg and his mentor Edward Tatum at Yale University in 1946 [15] discovered that bacterium *Escherichia coli* can exchange genetic information analogous to sexual reproduction. Conjugation — DNA being transfered between bacterial cells through direct cell-to-cell contact or by a bridge like structure, is the second mechanism of HGT. It has been shown conjugation can happen within a species as well as between species, and even kingdoms [16, 17].

The third mechanism of HGT is transduction, which describes the transfer of one bacterium host genomic DNA to a new host by a virus upon infection. It was discovered again by Joshua Lederberg, together with his graduate student Norton Zinder in 1952. They demonstrated bacteriophage P22 can carry genetic material from one strain of bacterium *Salmonella typhimurium* to another [18].

Driven by increasingly routine whole genome sequencing and partial sequencing of whole microbial communities (metagenomics), subsequent comparative genomics studies have revealed that bacterial genome plasticity in natural environments is extensive [19–21]. For prokaryotes, HGT facilitates genomic innovation [19, 21, 22] and compensates for the lack of sexual recombination, providing potential adaptive and selective advantage. Hence it is often referred to as "bacterial sex" [23]. HGT is facilitated through mobile genetic elements [24] including insertion sequences, transposons, integrons, genomic islands, and of particular interest to this work, plasmids and bacteriophage. These elements comprise the available pangenome [25] for HGT in an ecological community.

This thesis will focus mainly on conjugation. Conjugation was first observed in the gram negative species *E. coli* [15] and later in the gram positive species *Streptococcus faecalis* [26]. In gram positives, conjugation is triggered by pheromones, secreted from the recipient to the donor, which activate the genes on the conjugative plasmid to induce cell aggregation (review [27]). Unlike phage transduction which is limited by host-phage compatibility, conjugation is broad host compatible. Genomic evidence reveals DNA transfer between genera, phyla and even major domains [16, 28].

Plasmids, a term coined by Joshua Lederberg in 1952 [29], are circular pieces of extra chromosomal DNA which contain a replication origin to recruit to host polymerase for autonomous replication and copy number maintenance [30]. Plasmids vary greatly in size (lengths of 1–1000 kbp) and function, often containing genes involved in detoxication, virulence, ecological interactions, antibiotic resistance, and conjugation.

Conjugative plasmids [31] encode for the necessary component for mating pair formation and DNA transfer and are a powerful tool for genome evolution as they can harbor and transfer genes between organisms sampling all genomes within an ecosystem[32]. Conjugative plasmids are among the largest plasmids, generally in the range of 15–750 kbp). Some conjugative genes have also been found on transposons [33] though plasmid systems have been studied more extensively.

Numerous mechanisms are responsible for plasmid mobility. A recent analysis [34] of all publicly available plasmid sequences defined potential mobility by the presence of two elements, *oriT* (transfer origin) and a mobilization relaxase gene. Mobile plasmids may also contain a type IV secretion system coupling protein. However, for conjugation, the full type IV secretion system (T4SS) is required (recent reviews of T4SS diversity, functionality, and evolution [35–39]). The general mechanism of conjugation is highly conserved in both plasmids and transposon systems [39]. First the DNA substrate is processed by proteins that assemble around the origin of transfer (*oriT*), forming a complex called the relaxome. The relaxome complex then nicks and unwinds the DNA by binding to the 5' end of the *oriT* region. The DNA-relaxome complex is then recruited to the T4SS channel by ATPase homologues and is translocated.

Three types of T4SS have been described [39, 40]: i) mediators of conjugal DNA transfer between cells; ii) effector translocator systems which deliver proteins or other effector molecules to eukaryotic target cells; and iii) DNA release or uptake systems that translocate DNA to or from the extracellular domain. Both i) and ii) are important pathways for pathogenic organisms, with i) being the basis for genetic plasticity and ii)establishing host-pathogen interaction [41]. In the last ten years, considerable research has discovered the role of T4SS secreted effector molecules in the pathogenicity of *Helicobacter pylori, Bordetella pertussis, Bartonella Spp.* and the intracellular survival of *Legionella pneumophila, Brucella spp.* (reviewed in [4, 41]). However, the overwhelming concern in many hospitals is the possibility for acquired antibiotic resistance from T4SS conjugal plasmid transfer in both gram negative and gram positive species, for instance, *Enterococcus faecium* a gram positive vancomycin resistant donor, and methicillin resistant *Staphylococcus aureus*, which are rapidly acquiring vancomycin resistance [42, 43].

Cells containing the conjugative plasmid are referred to as donors, while the cells receiving the plasmid are termed recipients. Following mating pair formation, the conjugative plasmid is transferred to the recipient, thus enabling the recipient to become an active donor. The mating bridge also allows the two genomes to participate in sexual recombination [15] as well as transferring any smaller non-conjugative plasmids [44]. Like other plasmids, conjugative plasmids contain a replication origin (*oriV*), recruiting the host polymerases to replicate, and thus propagate the plasmid to daughter cells through replication as well. This muddles the boundary between proliferation and genetic exchange in prokaryotes [45].

1.3 Spontaneous Mutation

Although HGT is more widely studied in microbial communities, within a single lineage under selective pressure, spontaneous mutation can also be a powerful contributor by altering the sequence of DNA. Salvado Luria and Max Delbrück identified that genes can be spontaneously mutated in their famous 1943 Fluctuation Test experiment [46], and they were also the first to quantify the rate of spontaneous mutation

in bacteria.

Mutations happened within gene exons or regulatory elements can confer observable effects to organism's phenotype. Most spontaneous mutations are neutral (having no effect on the fitness of the organism) or deleterious (decreasing the fitness of the organism), and advantageous mutations (increasing the fitness of the organism) occur at a lesser frequency. The accumulation of spontaneous mutations can achieve an appreciable effect over a long period of time. For instance, sometimes point mutations (in the genome) can confer resistance to antibiotics, and long term (persistent) infections treated with multiple antibiotics (periods of selective pressure) show accumulation of multiple resistant point mutations [47] simply through their inherent mutagenesis rate and population size.

Mutation rate reflects the balance between maintaining the fidelity of DNA replication and the flexibility of adapting to changing environments. Mutation rate varies across species. With regards to an organism's "optimized" inherent mutation rate, there is a strong inverse correlation with genome size/complexity [48]. In *E. coli*, the spontaneous mutation occurs at a very low rate, which is less than 10^{-9} per base pair per replication [49].

Compared to a wild-type phenotype with low spontaneous mutation rate, a mutator phenotype has a much higher spontaneous mutation rate due to the defects in DNA replication/repair or protein translation systems [50, 51]. Of these systems, the methyl-directed mismatch-repair system (*mutS*, *mutL*, *mutH* and *uvrD*) has been found to be the most frequently affected in naturally mutator phenotypic bacterial populations [52, 53].

Under constant environment conditions, the increased mutation rate reduces the relative fitness of the mutator phenotype through the accumulation of deleterious mutations [54], and the wild-type strain with the lower mutation rate usually goes to fixation. However, in fluctuating conditions, analogous to "real" environments, the mutator phenotype can confer a fitness advantage through the increased probability of generating beneficial mutations. Adaptation occurs by introduction of a beneficial allele by mutation, and then selection for that allele drives fixation. When beneficial mutations occur, modifier alleles that raise

the mutation rate (mutator phenotype) can hitchhike to high frequency with them, thereby increasing the average mutation rate in the population [55–59].

In laboratory experiments, mutators can be selected and enriched for in conditions such as nutrient limitation or antibiotic stress, becoming dominant. Surprisingly, even in natural environments, mutators can sometimes represent as much as 15 % of the population [52, 60–62]. They have gained renewed interest due their prevalence in infectious disease [63–66] and implications towards cancer [67, 68].

Previous work in large experimental populations of bacteria has demonstrated that mutators can proliferate in association with new beneficial mutations [69, 70] if above a certain inoculation threshold (density dependence). Below this threshold, mutators will typically decline in frequency because wild-type are more likely to be associated with new beneficial mutations. However, when a large bacterial culture is exposed to multiple rounds of lethal selection, the frequency of clones bearing spontaneous mutator mutations within the culture can be greatly enhanced because these clones have a higher probability of producing mutants that survive the selection [71]. Recent modeling using temporal fluctuations in selection [72, 73] have found that even very small initial populations of mutators can become fixed.

2

Conjugation

As much of our modern laboratory molecular biology and genetic engineering rely on the use of plasmids, we still lack full understanding of plasmid dynamics to eliminate the uncontrolled spread of undesired genes through plasmid-based horizontal gene transfer. To understand the transfer, maintenance and loss of plasmids, numerous interesting mathematical models [74–81] to describe plasmid conjugation have been developed over the past decade, where the experimental validation relied on quantifying the number of functional transconjugants through selective culturing. This strategy has at least two shortcomings: selective culturing introduces the contribution of selection pressure and fitness; it is difficult to

parse the transfer rate of the plasmid from the additional mechanistic steps involved in the formation of functional transconjugants. A clever alternative to selective culturing is the use of donor-suppressed fluorescent reporter genes [82, 83], which upon transfer, create fluorescent recipients. Although reporter genes like green fluorescent protein are functional in a broad number of species, the production of nonessential proteins can also be a metabolic burden, again creating a selection pressure.

To overcome these problems, this chapter presents a novel quantitative polymerase chain reaction (qPCR) assay to directly measure the plasmid transfer through the relative abundance of carefully chosen genetic loci. This method not only improves the reproducibility and signal-to-noise level through qPCR's single molecule (loci target) sensitivity, but also avoids adding selective factors by eliminating measurement's dependence on culturing.

I will first demonstrate the effectiveness of using qPCR to track the growth of different genetic markers (loci) within a homogeneous (clonal) population in real time in a batch culture. Unlike the bio-reactor continuous culture experiments, the batch culture is a natural limitation to impose a resource constraint resembling "real" environment.

I will then extend the study to a population of cells with an inhomogeneous initial distribution of a genetic marker which can be exchanged between a donor and a recipient bacterium. In the model bacterium, *Escherichia coli*, this process is enabled by a series of genes encoded on an independently replicating minichromosome called the F plasmid [29]. Conjugation commences when the tips of F pili from a donor cell (termed F+) make contact with recipient cells (F-) [31, 32] creating a mating bridge. Recent work has shown the pili to be a dynamic structure, extending and retracting continuously [84]. When the pili retract, the cells form a mating pair aggregate [85]. Though the process of conjugation in *E.coli* has been studied since the 1950s, all prior experiments required selective culturing prior to enumeration. Our qPCR method does not require selective culturing, thus enabling the study of bacterial conjugation process in the absence of selective pressure.

I initially hoped to investigate this model conjugation system in both positive and negative selection

conditions. Ironically, I found that the rate of conjugation was comparable to the encounter rate of bacteria (see Section 2.4). Hence, it was impossible to expand the study to measure the influence on the kinetics of a positive selective force (e.g. acquired antibiotic resistance). However, the maintenance of "sexuality" comes at a metabolic cost to the bacterium as well as making the cell venerable to viral attacks. Bacterial viruses, or bacteriophage, are specific to the conjugation machinery, infiltrating the cell and hijacking the metabolism for replication of viral particles. Therefore, it is surprising that the genes enabling conjugation persist in the environment if they are not conferring a benefit above those costs of maintaining the conjugative genes.

I will once again use the qPCR assay to elucidate the kinetic influence of a filamentous phage specific to the conjugation machinery, M13, on the growth of the host cell. Filamentous phage do not kill their host, and the infected cells continue to grow and divide indefinitely while producing new phage particles. M13 phage do not form in the cytoplasm; rather they are continually extruded or secreted across the bacterial membranes as they are assembled, without causing cell lysis [86]. Since M13 phage do not lyse the host, it has become a popular model system for studying chronic infection.

Finally, I will investigate how M13 phage infection affects the dynamics of plasmid conjugation between donor (F+) and recipient (F-) cells. By quantifying phage's impact on conjugation, one can derive a regime in which phage therapy could be a viable option to treat the spread of antibiotic resistance through plasmid conjugation.

2.1 Materials and Methods

2.1.1 Strains

E. coli strain W6 (F+, *relA1*, *spoT1*, *metB1*, *rrnB-2*, *creC510*)(CGSC 4427) was used as donor in conjugation experiment. For recipient, a W6 (F-) strain was created by curing W6 (F+) with a modified acridine orange protocol: W6 (F+) cells were grown overnight in Luria broth supplemented with 80 μg mL^{-1} acridine or-

ange at 37 °C (details in [87, 88]). The loss of F plasmid was confirmed by the loss of *traI* qPCR signal (see Section 2.1.3). Following curing, an essential F plasmid replication gene *rpoH* was sequenced to assure the absence of unintended secondary mutations.

The M13 bacteriophage (ATCC 15669-B1) were revived before each growth experiment (see Section 2.1.2 for phage revival details).

2.1.2 Growth Assays

The growth assays differed based on the four tested conditions: **1)** pure culture growth; **2)** conjugation; **3)** phage infection; **4)** conjugation under phage infection. I have chosen conditions of each growth experiment to measure selected mathematical model parameters, thus reducing the number of unknown parameters in the final complete model (see Section 2.2 for details of the model).

Single colonies of W6 (F+) and W6 (F-) cells were inoculated into separate glass tubes containing 5 mL Luria broth, and grew at 37 °C overnight.

M13 phage were revived by mixing with exponential growth phase W6 (F+) cells in 3 mL Luria broth and allowed to grow overnight at 37 °C. 1 mL of the overnight culture was centrifuged at 12 000 rpm for 10 min (Eppendorf Centrifuge 5417R; Eppendorf AG, Hamburg, Germany). The fresh supernatant containing the revived M13 phage was collected for growth experiment. It has long been understood that phage infection inhibits the growth of *E.coli* cells, hence it is possible to visualize translucent phage plaques against a saturated *E. coli* lawn in top agar. Prior to each growth experiment, the phage were titered on W6 (F+) lawns to quantify the viable concentration used in each experiment.

Common to all tested conditions, inoculum subcultures of pure or mixed cell populations were prepared in a 1.7 mL tube, then the volume specified in each condition was used inoculating 50 mL preheated 37 °C Luria broth in 250 mL flasks.

Condition 1) pure culture growth: The overnight W6 (F+) cultures was used as inoculum.

Condition 2) conjugation: The overnight W6 (F+) and W6 (F-) cultures were mixed in ratios of F+:F- (1:1(500 µL:500 µL), 1:10(100 µL:1000 µL), 1:10^2(10 µL:1000 µL), 1:10^3(1 µL:1000 µL)). 200 µL of each mixture was then used as inoculum.

Condition 3a) phage infection — varying cell inoculum concentration: 500 µL of ten-fold serial dilutions (1, 10^{-1} and 10^{-2})were prepared from overnight W6 (F+) culture. Each serial dilution was then mixed with 5 µL freshly revived M13 phage (titer $\sim 10^{11}$ mL^{-1}). The full volume of the mixture (505 µL was then used as inoculum.

Condition 3b) phage infection — varying phage inoculum concentration: Ten-fold serial dilutions were prepared from freshly revived phage supernatant (1, 10^{-1}, 10^{-2}, 10^{-3} and 10^{-4}). 50 µL of each phage dilution was mixed with 50 µL W6 (F+) cells, and the full volume of the mixture (100 µL) was used as inoculum.

Condition 4) conjugation under phage infection: W6 (F+) and W6 (F-) mixtures of different ratios were prepared by following **condition 2)**. 200 µL of each mixture was then used as inoculum. Right after inoculation of cell mixtures, each flask was inoculated with 5 µL freshly revived M13 phage culture (titer $\sim 10^{11}$ mL^{-1}).

Flasks were then incubated in a water bath immersion shaker (model G67; New Brunswick Scientific, New Brunswick, NJ), shaking at 110 rpm, and maintained at 37 °C. The rate of mating pair formation has been shown to be constant over a broad range of shake flask shear forces (0 to 300 rpm) [81]. 100 µL aliquots were extracted every 15 or 20 min without pausing the shaking or removing the flask from the immersion bath. The 100 µL aliquot was diluted with 400 µL water (Millipore - MilliQ RO purified), then placed in a 95 °C dry bath to lyse the cells (preserving the cell number and denaturing potential degradation enzymes). Aliquots were then stored at −20 °C until their use as template for the qPCR assays.

2.1.3 Quantitative PCR Assay

Quantitative PCR is routinely used for quantifying targeted DNA abundance. It allows for the enumeration of a targeted genetic marker (DNA or RNA) at unrivaled sensitivity (single copy number) through optimization.

All qPCR reactions used a master mix consisting of the following: 2 mM $MgCl_2$, 200 µM of each dNTP, 1U (per 25 µL volume) Roche FastStart Enzyme blend (Roche Diagnostics, Mannheim, Germany), 1X Roche FastStartBuffer (Roche Diagnostics), 0.4 µM forward and reverse primers (see Table 2.1 for primer details), 2 µM SYTO 9 green fluorescent nucleic acid stain (Invitrogen; Life Technologies, Carlsbad, California), and 1X ROX reference dye (Invitrogen; Life Technologies). Instead of more widely used SYBR Green dye, SYTO 9 dye is used for double stranded DNA quantification as it has been shown to have less sequence and concentration artifacts [89]. 5 µL lysed frozen aliquots from growth experiments were used as template for a 25 µL qPCR reaction.

All reactions were performed in a BioRad Chromo4 Instrument (Bio-Rad Laboratories, Hercules, CA), in 96 well, clear bottom, hard shell, skirted assay plates (Bio-Rad Laboratories) with Microseal B sealing tape (Bio-Rad Laboratories). The instrument filter was set to FAM for SYTO9. When ROX was used as a passive reference dye, additional filter ROX was also set. Thermal cycles used are following: one cycle of 95 °C for 6 min, followed by 35 cycles of 95 °C for 30 s, 50 °C for 30 s, plate read, and 72 °C for 25 s.

Table 2.1: Primers used in conjugation study

Primers	$5' \rightarrow 3'$
tolC Forward	CGACAAACCACAGCCGGTTA
tolC Reverse	CAGCGAGAAGCTCAGGCCA
traI Forward	GCCATTCATCTTGCCCTTCC
traI Reverse	GCATGACCGCCTCCTTACC
M13 Forward	TTGTTCCTTTCTATTCTCACTCC
M13 Reverse	CACCCTCAGAACCGCCACC

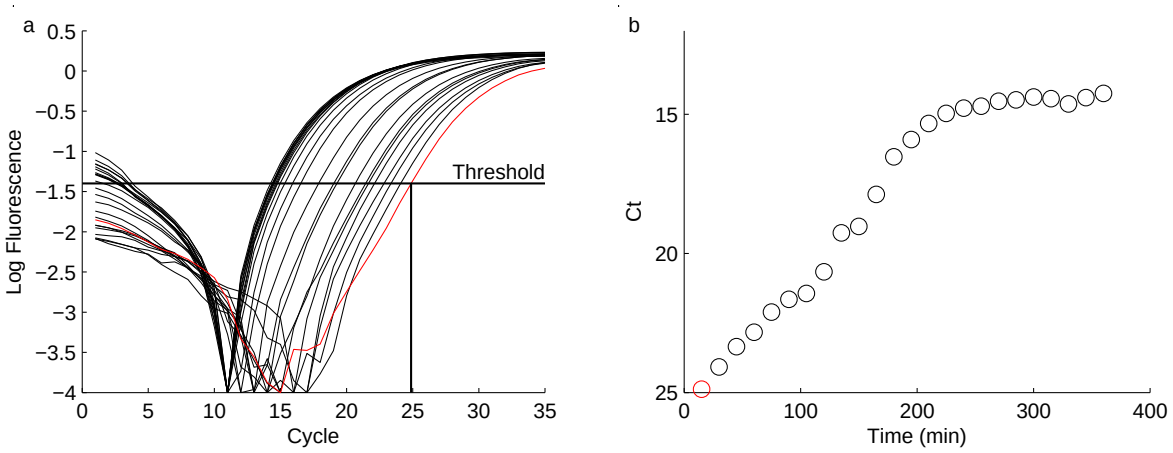

Figure 2.1: (a) Log plot of the fluorescent signal of amplification curves from 24 qPCR reactions. The threshold cycle (Ct) of a specific reaction is the cycle number at which the of the amplification curve intersects the threshold line. The red amplification curve show one example of determine Ct of that specific reaction. (b) The Ct value is inversely related to the amount of starting template. A plot of the Ct values versus time yields the growth curve for the targeted locus. The red circle corresponds to the red amplification curve of subplot a

Figure 2.1a shows the output of a qPCR growth assay. The fluorescent signal of amplification curves is proportional to the amount of double stranded DNA (dsDNA) product. The relative abundance of starting template can be quantified by the time elapsed for the amplification curve to intersect with the florescent signal threshold (labeled as threshold in Figure 2.1a). Usually the threshold is chosen to intersect amplification curves during exponential phase (linear phase in Figure 2.1a because the fluorescence is plotted in log scale). As the cell population grows, the number of targeted locus DNA grows proportionally. Therefore samples collected at later time points should have larger amount of template DNA compared to those collected at early timer points. As the amount of starting template DNA increases, the time necessary to reach the threshold value decreases. The threshold values, C_t, can be translated into a growth curve (Figure 2.1b) by plotting the C_t value of each amplification curve from Figure 2.1a versus its corresponding sample collecting time point.

The starting template DNA concentration, n, can be converted to C_t values as following:

$$C_t = C_{to} - \log_2 n \tag{2.1}$$

where C_{to} is an arbitrary constant determined by best fitting qPCR data. The single copy chromosomal gene *tolC* was found in both plasmid-bearing (F+) and plasmid-free (F-) cells, but the single copy plasmid gene *traI* was only found in the plasmid-bearing (F+) cells. Therefore $C_t(\text{tolC})$ should correspond to the total number of F+ and F- cells, while $C_t(\text{traI})$ should only correspond to the number of F+ cells. Another single copy gene was chosen to track M13 phage, and $C_t(\text{M13})$ should correspond to the number of M13 phage particles.

$$C_t(\text{tolC}) = C_{to} - \log_2(n_{\text{F+}} + n_{\text{F-}}) \tag{2.2}$$

$$C_t(\text{traI}) = C_{to} - \log_2(n_{\text{F+}}) \tag{2.3}$$

$$C_t(\text{M13}) = C_{to} - \log_2(n_{\text{M13}}) \tag{2.4}$$

where $n_{\text{F+}}$, $n_{\text{F-}}$ and n_{M13} represent the number of F+ cells, F- cells and M13 phage respectively.

One can see from Figure 2.2, the error in duplicate qPCR reactions using the same template (frozen cell aliquots from a single growth assay) is less than one cycle, including the error in the saturated phase. This means the error of qPCR is less than two fold, which is much more accurate compared to traditional plate colony counting technique.

2.2 Mathematical Model

Our resource-limited mass-action model was based on a series of papers that Bruce Levin and colleagues developed to study the dynamics of conjugation and the effect of M13 phage infection on conjugation process[90–93].

During conjugation, recipient cells (R) receive a copy of plasmid from donor cells (D) and become transconjugant cells (T), whereas donor cells become temporarily exhausted donor cells (X). The delays

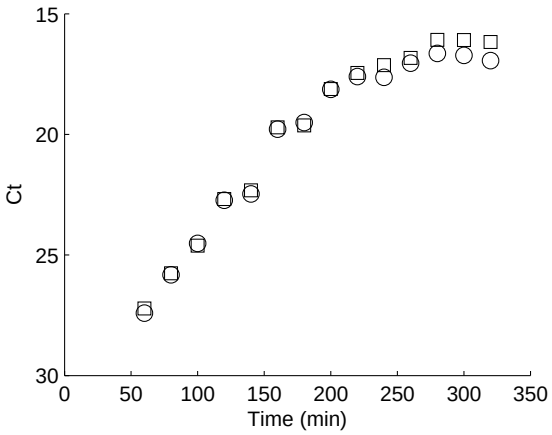

Figure 2.2: Circles and squares represent duplicate qPCR reactions using the same frozen cell aliquots of a single growth assay time series. As one can see the difference between duplicate qPCR reactions is less than one cycle

in transconjugant cells and temporarily exhausted donor cells becoming active donor cells are $1/\lambda_T$ and $1/\lambda_X$ respectively.

The interaction kinetics becomes more complex with the addition of phage. As M13 phage (P) is a F+ specific phage, because it can only infect plasmid-bearing donor cells (D) by binding to the tips of F+ cells' pili. Newly infected cells (N) cannot produce phage immediately, hence I introduce a lag time of $1/\lambda_N$ to account for the delay in becoming active phage-producing infected cells(I).

When M13 phage (P) are introduced into a mixture of donor (D) and recipient (R) cells, there is competition between conjugation and phage infection. Infected cells (N) can still conjugate, and become temporarily exhausted infected cells (XI), assuming they have the same lag time of $1/\lambda_X$ as uninfected cells to be able to conjugate again.

A schematic of phage and cells' various states, including all transition pathways, are shown in Figure 2.3. For easy reference, all symbols used in conjugation model are summarized in Table 2.2. The dynamics of resource consumption and each cellular state can be described by the following ordinary differential

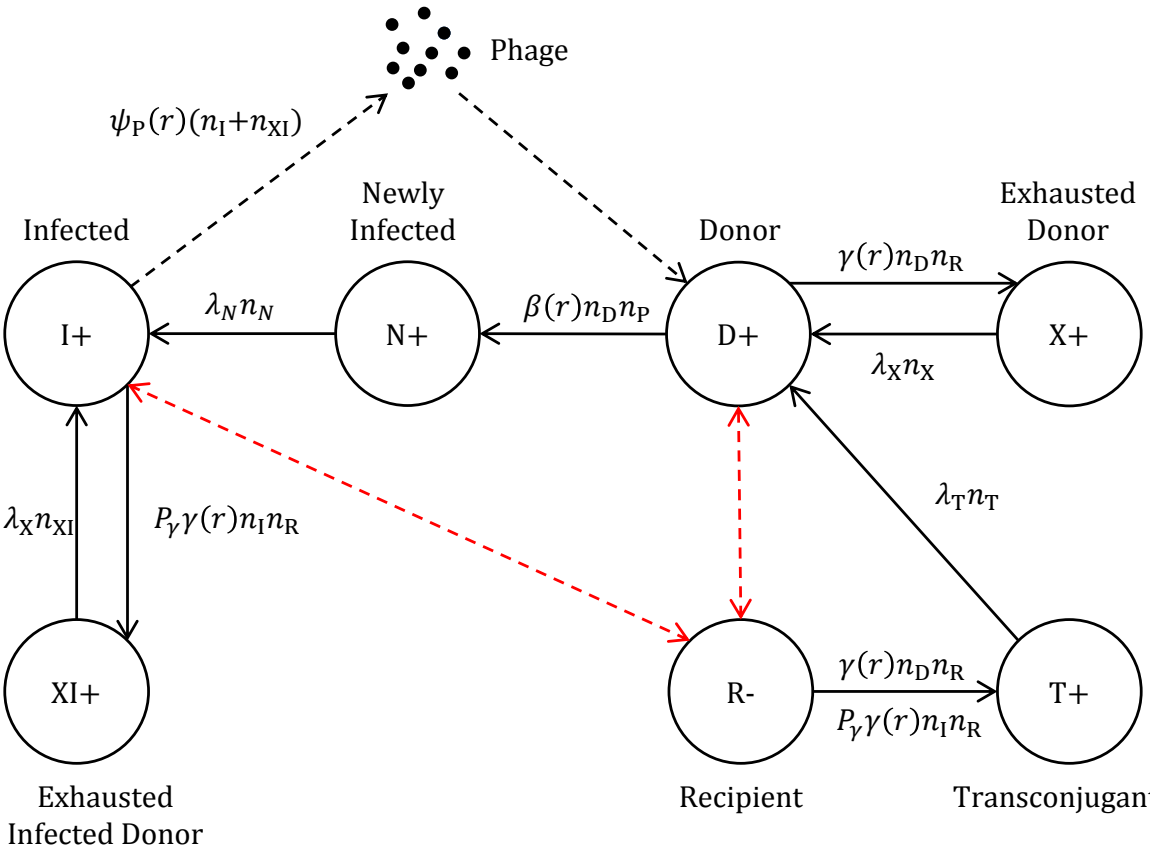

Figure 2.3: Schematic of all allowed transitions between cellular states during conjugation under phage infection used in the mathematical model. Each node represents a cellular state with its abbreviation in the node center followed by + or - representing plasmid-bearing and plasmid-free respectively. Black arrows denote the transitions between cellular states with specified transition rates. Black dashed arrows denote phage production and infection. Red dashed two-way arrows point to celluar states where conjugation happens

Table 2.2: Symbols used in conjugation model

Symbols	Physical Quantity
n_D	Density of donor cells (F+)
n_R	Density of recipient cells (F-)
n_X	Density of exhausted donor cells (F+)
n_T	Density of transconjugant cells (F+)
n_N	Density of newly infected cells (F+)
n_I	Density of infected cells (F+)
n_{XI}	Density of exhausted infected donor cells (F+)
n_P	Density of M13 phage
n	Density of all cells $n = n_D + n_R + n_X + n_T + n_N + n_I + n_{XI}$
r	Resource concentration
e	Resource consumption per cell division
Q	Concentration of resource when rate is half-maximum
K	Cell carrying capacity
K_P	Phage carrying capacity
$\psi(r)$	Resource-dependent cell growth rate
$\gamma(r)$	Resource-dependent conjugation rate
$\beta(r)$	Resource-dependent phage infection rate
$\psi_P(r)$	Resource-dependent phage production rate
ψ_{MAX}	Maximum cell growth rate
γ_{MAX}	Maximum conjugation rate
β_{MAX}	Maximum phage infection rate
$\psi_{P\,MAX}$	Maximum phage production rate
$1/\lambda_T$	Delay time in transconjugant cells becoming donor cells
$1/\lambda_X$	Delay time in (infected) exhausted donor cells becoming (infected) donor cells
$1/\lambda_N$	Delay time in newly infected cells becoming phage-producing infected cells
P_ψ	Penalty factor of cell growth rate due to phage infection
P_γ	Penalty factor of conjugation rate due to phage infection

equations:

$$\frac{dr}{dt} = -e\psi(r)(n_D + n_R + n_T + n_X)(1 - \frac{n}{K}) - eP_\psi\psi(r)(n_N + n_I + n_{XI})(1 - \frac{n}{K}) \quad (2.5)$$

$$\frac{dn_D}{dt} = \psi(r)n_D(1 - \frac{n}{K}) - \gamma(r)n_D n_R + \lambda_X n_X + \lambda_T n_T - \beta(r)n_D n_P \quad (2.6)$$

$$\frac{dn_R}{dt} = \psi(r)n_R(1 - \frac{n}{K}) - \gamma(r)n_D n_R - P_\gamma\gamma(r)n_I n_R \quad (2.7)$$

$$\frac{dn_T}{dt} = \psi(r)n_T(1 - \frac{n}{K}) + \gamma(r)n_D n_R - \lambda_T n_T + P_\gamma\gamma(r)n_I n_R \quad (2.8)$$

$$\frac{dn_X}{dt} = \psi(r)n_X(1 - \frac{n}{K}) + \gamma(r)n_D n_R - \lambda_X n_X \quad (2.9)$$

$$\frac{dn_N}{dt} = P_\psi\psi(r)n_N(1 - \frac{n}{K}) + \beta(r)n_D n_P - \lambda_N n_N \quad (2.10)$$

$$\frac{dn_I}{dt} = P_\psi\psi(r)n_I(1 - \frac{n}{K}) + \lambda_N n_N - P_\gamma\gamma(r)n_I n_R + \lambda_X n_{XI} \quad (2.11)$$

$$\frac{dn_{XI}}{dt} = P_\psi\psi(r)n_{XI}(1 - \frac{n}{K}) + P_\gamma\gamma(r)n_I n_R - \lambda_X n_{XI} \quad (2.12)$$

$$\frac{dn_P}{dt} = \psi_P(r)(n_I + n_{XI})(1 - \frac{n_P}{K_P}) \quad (2.13)$$

Equation (2.5) describes the rate of all cellular states (nodes in Figure 2.1) consuming resource r throughout growth until saturation. In resource-limited batch culture growth, cells follow logistic growth characterized by the term $1 - \frac{n}{K}$, in which n is the total cell density and K is the cell carrying capacity. Cells stop multiplying when resource is depleted or cell carrying capacity is reached. The cell growth rate is represented by $\psi(r)$ while $P_\psi$represents the growth penalty of phage infected cells. Both infected and uninfected cells utilize resource at the rate of e per cell division. Uninfected cellular states are described by their respective density: donors, n_D, recipients, n_R, transconjugants, n_T, and exhausted donors, n_X. Only functional donors can be infected by M13 (represented by the arrow from D+ to N+), and the related infected states are described also by their respective density: newly infected cells, n_N, infected cells, n_I, exhausted infected donor cells, n_{XI}, and phage, n_P.

Equations (2.6) to (2.12) describe the growth of all cellular states. All growth rates also have to take tran-

sitions between different cellular states into consideration. There are two kinds of transitions represented by first order and second order terms. First order terms represent the transition between inactive and active conjugation and phage production states, and the associated rate constants: λ_T, λ_X and λ_N , which are resource independent. Their reciprocals can be interpreted as delay time in transconjugant cells becoming donor cells, (infected) exhausted donor cells becoming (infected) donor cells, and newly infected cells becoming phage-producing infected cells respectively. Second order terms represent conjugation and phage infection, and the associated rate constants $\gamma(r)$ and $\beta(r)$ are resource dependent. P_γ represent the penalty factor of conjugation rate due to phage infection.

Equation (2.13) describes the phage production of infected cells. It follows a similar form of cell growth with resource-dependent production rate of $\psi_P(r)$, and phage carrying capacity of K_P.

Jacques Monod proposed that bacterial growth kinetics resemble enzyme kinetics in terms of substrate limitation [94], an idea that was further refined for modeling conjugative transfer as a Michaelis-Menten kinetic scheme [74]. Similarly one can assume the cell growth rate $\psi(r)$, conjugation rate $\gamma(r)$, phage infection rate $\beta(r)$ and phage production rate $\psi_P(r)$ all follow a hyperbolic form similar to Michaelis–Menten kinetics in terms of resource concentration:

$$\psi(r) = \frac{r\psi_{MAX}}{Q+r} \tag{2.14}$$

$$\gamma(r) = \frac{r\gamma_{MAX}}{Q+r} \tag{2.15}$$

$$\beta(r) = \frac{r\beta_{MAX}}{Q+r} \tag{2.16}$$

$$\psi_P(r) = \frac{r\psi_{P\,MAX}}{Q+r} \tag{2.17}$$

where the subscript MAX denotes the rate maximum, and Q denotes the resource concentration when the rate is half-maximum.

2.3 Results

All simulations were performed using MATLAB. During simulation, Equations (2.5) to (2.13) were simplified according to growth assay conditions, and parameters values were optimized relying on the method of least squares regression.

2.3.1 Pure Culture Growth

For growth assay **Condition 1) pure culture growth**, Equations (2.5) to (2.6) can be simplified as

$$\frac{dr}{dt} = -e\psi(r)n_{\mathrm{D}}(1 - \frac{n}{K}) \tag{2.18}$$

$$\frac{dn_{\mathrm{D}}}{dt} = \psi(r)n_{\mathrm{D}}(1 - \frac{n}{K}) \tag{2.19}$$

Carrying capacity K

I estimated the order of magnitude for the carrying capacity, K, in Luria broth by counting the number of cells at saturation using a hemocytometer. The estimated $K \sim 10^9$ mL^{-1} value has been cross validated by counting viable colony on Luria broth plates. The estimated value was used as initial value for least squares regression. The optimization yielded the value of carrying capacity in Luria broth $K = 3.5 \times 10^9$ mL^{-1}.

Maximum growth rate $\psi_{\mathbf{MAX}}$

To extract the maximum growth rate, by following growth assay **Condition 1)**, a pure culture of F+ cells was grown and the time series samples were tested for the abundance of *tolC* and *traI* loci. Mating between F+ cells is unlikely due to surface exclusion mechanisms encoded by *traS* and *traT* genes [95]. It was found the growth (Figure 2.4) of the *tolC* (circle) and *traI* (square) loci were maintained at a ratio of approximately 1:1 throughout the batch growth process, consistent with the previous observations of one F plasmid per

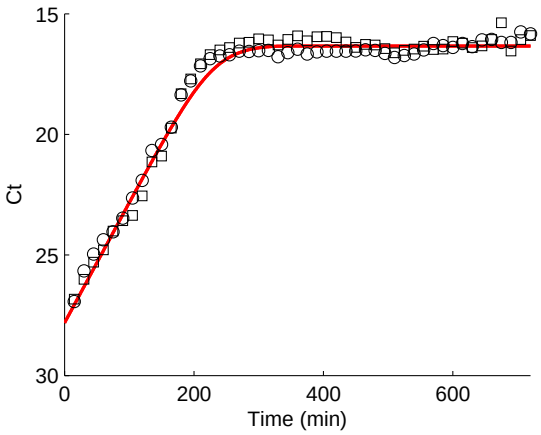

Figure 2.4: Time series plot of *tolC* (circle) and *traI* (square) for a pure F+ culture. Red line represents the fitted curve

cell. Hence, one can infer that cellular replication is the underlying mechanism increasing the abundance of both loci. The maximum growth rate, $\psi_{\text{MAX}} = 0.035\ \text{min}^{-1}$ can be extracted from Figure 2.4 by fitting the exponential phase.

Resource consumption per cell division e and resource concentration when rate is half-maximum Q

Since r scales with e (Equation (2.5)), both parameters were defined in terms of arbitrary units (a.u.). Again, the growth of pure F+ culture (Figure 2.4) was used for these estimates. Equation (2.14) relates $Q = 1$ a.u. and $r = 100$ a.u. to the maximum growth rate $\psi_{\text{MAX}} = 0.035\ \text{min}^{-1}$. Using Equation (2.5) under these constraints enables us to find $e = 3.5 \times 10^{-8}$ a.u. mL. Values of e have been reported for defined glucose supplemented minimal media [93]. However, Luria broth, the common laboratory media for rapid growth of *E. coli* cultures, is not supplemented with glucose. Growth has been shown to be limited by the utilization of catabolizable amino acids [96].

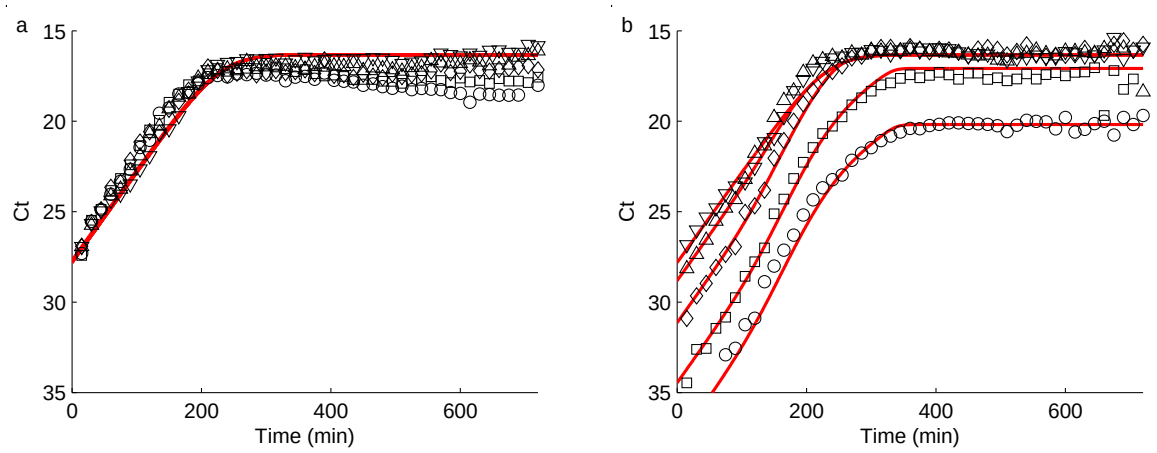

Figure 2.5: Simulation (solid red line) and qPCR data (symbols) of time series plots of *tolC* (a) and *traI* (b) for conjugation between F+ and F- cells. Each plot represents a different inoculation ratio of F+ to F- cells: pure F+ (donor) culture (downward-pointing triangle)(same as Figure 2.4), 1:1 (upward-pointing triangle), 1:10 (diamond), $1{:}10^2$ (square), and $1{:}10^3$ (circle)

2.3.2 Conjugation

For the growth assay **Condition 2) conjugation**, Equations (2.5) to (2.9) can be simplified as

$$\frac{dr}{dt} = -e\psi(r)(n_D + n_R + n_T + n_X)(1 - \frac{n}{K}) \tag{2.20}$$

$$\frac{dn_D}{dt} = \psi(r)n_D(1 - \frac{n}{K}) - \gamma(r)n_D n_R + \lambda_X n_X + \lambda_T n_T \tag{2.21}$$

$$\frac{dn_R}{dt} = \psi(r)n_R(1 - \frac{n}{K}) - \gamma(r)n_D n_R \tag{2.22}$$

$$\frac{dn_T}{dt} = \psi(r)n_T(1 - \frac{n}{K}) + \gamma(r)n_D n_R - \lambda_T n_T \tag{2.23}$$

$$\frac{dn_X}{dt} = \psi(r)n_X(1 - \frac{n}{K}) + \gamma(r)n_D n_R - \lambda_X n_X \tag{2.24}$$

Maximum conjugation rate γ_{MAX}

Figure 2.5 shows the time series of *tolC* (Figure 2.5a) and *traI* (Figure 2.5b) loci in conjugation experiments described in growth assay **Condition 2)**. Each plot represent a specific ratio of F+ to F-: 1:1 (upward-

pointing triangle), 1:10 (diamond), $1:10^2$ (square), and $1:10^3$ (circle). For comparison, the pure F+ culture data (from Figure 2.4) is also shown in Figure 2.5 as downward-pointing triangles.

One can easily observe the rate of growth for the chromosomal *tolC* loci (Figure 2.5a) is similar across all mixtures as well as the pure F+ culture. However when examining the rate of growth of the plasmid *traI* loci (Figure 2.5b), the exponential phases all differ from the growth of the pure F+ culture, reflecting the contribution of conjugation events.

The solid red lines shown are plots of simulation results. I allowed the least squares algorithm to search for the best values, starting from our estimates of K, ψ_{MAX}, e and Q from above discussions and the reported values for λ_{T} and λ_{X} [74, 97]. I found the maximum plasmid transfer rate in uninfected cells to be $\gamma_{\text{MAX}} = 3 \times 10^{-10}$ mL min^{-1}.

2.3.3 Phage Infection

For the growth assay **Condition 3) phage infection**, Equations (2.5), (2.6), (2.10), (2.11) and (2.13) can be simplified as

$$\frac{dr}{dt} = -e\psi(r)n_{\text{D}}(1-\frac{n}{K}) - eP_{\psi}\psi(r)(n_{\text{N}}+n_{\text{I}})(1-\frac{n}{K}) \tag{2.25}$$

$$\frac{dn_{\text{D}}}{dt} = \psi(r)n_{\text{D}}(1-\frac{n}{K}) - \beta(r)n_{\text{D}}n_{\text{P}} \tag{2.26}$$

$$\frac{dn_{\text{N}}}{dt} = P_{\psi}\psi(r)n_{\text{N}}(1-\frac{n}{K}) + \beta(r)n_{\text{D}}n_{\text{P}} - \lambda_{\text{N}}n_{\text{N}} \tag{2.27}$$

$$\frac{dn_{\text{I}}}{dt} = P_{\psi}\psi(r)n_{\text{I}}(1-\frac{n}{K}) + \lambda_{\text{N}}n_{\text{N}} \tag{2.28}$$

$$\frac{dn_{\text{P}}}{dt} = \psi_{\text{P}}(r)n_{\text{I}}(1-\frac{n_{\text{P}}}{K_{\text{P}}}) \tag{2.29}$$

Phage carrying capacity K_{P}

As mentioned in growth assay, a standard plaque assay was used to estimate the phage carrying capacity. At the beginning of each growth experiment, phage were also titered on W6 (F+) lawns to quantify the

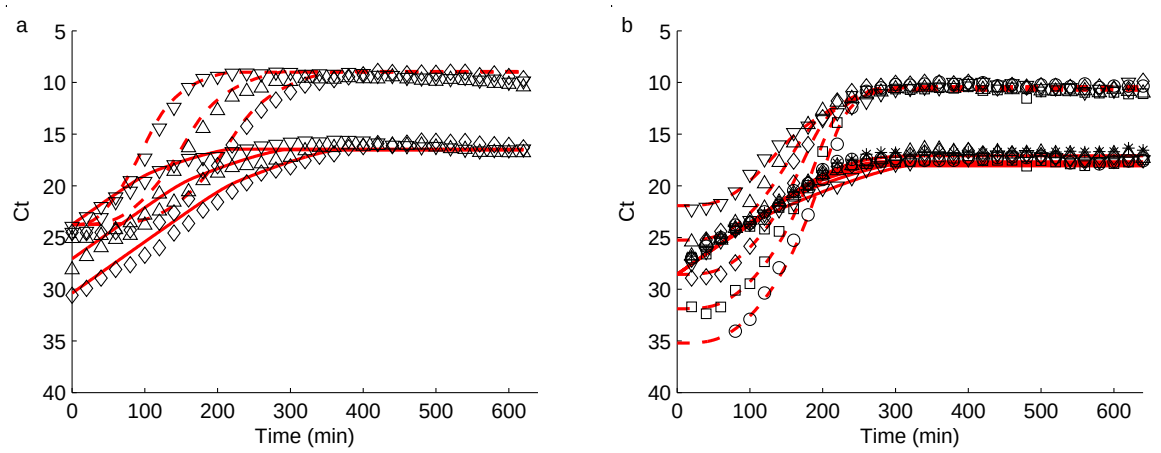

Figure 2.6: (a) Different concentrations of cells (*tolC* locus (solid red line)) infected by the same concentration of phage (red dotted line) at ratio of 1:1 (downward-pointing triangle), 10^{-1}:1 (upward-pointing triangle), 10^{-2}:1 (diamond). (b) The same concentration of cells (*tolC* locus (solid red line)) infected by different concentrations of phage (red dotted line) at ratio of $1{:}10^{2}$ (downward-pointing triangle), 1:10 (upward-pointing triangle), 1:1 (diamond), $1{:}10^{-1}$ (square), and $1{:}10^{-2}$ (circle)

viable concentration used in each experiment. The values from various experiments gave the estimation of $K_P \sim 10^{11}$ mL^{-1} was used as the initial parameter value for following least square optimization. The final optimized value is $K_P = 4 \times 10^{11}$ mL^{-1}.

Maximum phage infection rate β_{MAX}, maximum phage production rate $\psi_{P\,MAX}$ and penalty factor of cell growth rate due to phage infection P_ψ

To assess the phage infection rate and production rate, pure F+ cultures were inoculated with M13 with two different experimental conditions to extract phage related parameters. Figure 2.6a shows the result of growth assay **Condition 3a)** with different cell inoculum concentrations (1 (downward-pointing triangle), 10^{-1} (upward-pointing triangle), 10^{-2} (diamond)). Figure 2.6b shows the result of growth assay **Condition 3b)** with different phage inoculum concentrations(1 (downward-pointing triangle), 10^{-1} (upward-pointing triangle), 10^{-2} (diamond), 10^{-3} (square), and 10^{-4} (circle)).

To find the growth penalty factor P_ψ, the *tolC* locus data from Figure 2.6 can be fitted with the adjusted

growth rate $P_\psi\psi(r)$, revealing a value $p_\psi = 0.6$. This implies that infection reduces the maximum growth rate to 60 % of its original value.

Newly infected cells have a latent period of 30 minutes before they begin to excrete phage [98], and this value was used in this model. From Equation (2.13) one can see phage are produced at rate of $\psi_{\mathrm{P}}(r)$ per infected cell. Fitting the data from Figure 2.6 yields maximum phage production rate $\psi_{\mathrm{P\,MAX}} = 6\,\mathrm{min}^{-1}$ by each infected cell. F+ donor cells are infected at a rate of $\beta(r)n_{\mathrm{D}}n_{\mathrm{P}}$ as stated in Equation (2.6). Using all the previously fixed values, one can again fit the phage data (red dotted line) in Figure 2.6 to find the maximum phage infection rate $\beta_{\mathrm{MAX}} = 3 \times 10^{-11}\,\mathrm{mL\,min}^{-1}$.

2.3.4 Conjugation under Phage Infection

For growth assay **Condition 4) conjugation under phage infection**, the complete mathematical model of Equations (2.5) to (2.13) has to be used.

Penalty factor of conjugation rate due to phage infection P_γ

Finally, to test the effect of phage infection on conjugation, growth assay **Condition 4)** was carried out and the resulting growth data are shown in Figure 2.7. Figure 2.7a displays the chromosomal *tolC* locus, Figure 2.7b the F plasmid *traI* locus, and Figure 2.7c the M13 phage. Simulations are shown as solid lines through the data points. The contributions to each node in the mathematical model are now much more complex, with every node and transition in Figure 2.3 represented. By using parameters found from the previous growth assay **Condition 1) to 3)** in the complete model (Equations (2.5) to (2.13)) to fit the penalty factor associated with the inhibition of conjugation, yields $P_\gamma = 0.1$, meaning the conjugation rate is reduced to 10 % of its maximum rate . This value is smaller but comparable to the reported value that finds the average rate reduced by 5 fold [99]. However, unlike the good fits to the previously presented data, there is a strong deviation from the model for phage production in Figure 2.7c at later time points.

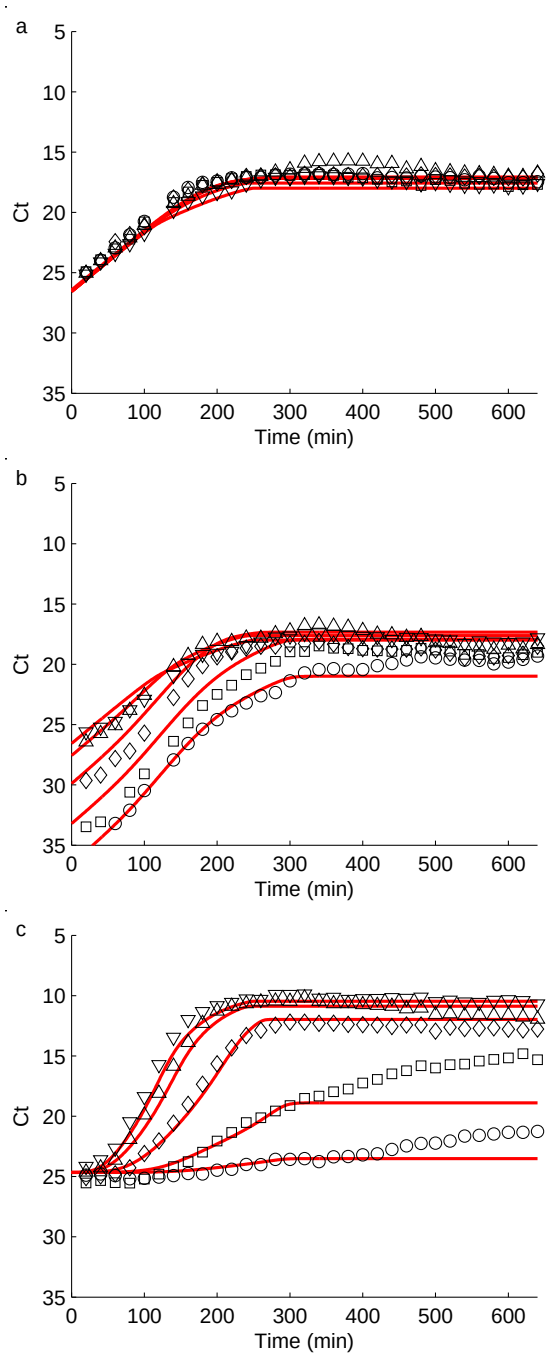

Figure 2.7: (a)*tolC*, (b)*traI* and (c)M13 simulation (red solid line) and qPCR data (closed symbol) of conjugation under phage infection time series. Each plot represents a different inoculation ratio of F+ to F- cells: pure F+ (downward-pointing triangle), 1:1 (upward-pointing triangle), 1:10 (diamond), $1{:}10^2$ (square), and $1{:}10^3$ (circle)

The model appears to be in good agreement for large initial F+ concentrations but deviates when the F+:F- ratio is $1{:}10^2$ or below.

2.4 Discussion

This chapter presented a novel method to measure the population abundance of mixed cultures by enumerating the temporal growth of individual genetic loci in a qPCR assay. By separating measuring from culturing, I reduced the error associated with selective culture screening. By lysing all samples immediately after collection, I also greatly reduced the sampling error. By relying on the precision of qPCR, I obtained high quality data for accurate downstream modeling and simulation. Parameters used in conjugation model simulation are summarized in Table 2.3.

Table 2.3: Parameter values used in conjugation model

Physical Quantity	Value
r	100 a.u.
e	3.5×10^{-8} a.u. mL
Q	1 a.u.
K	3.5×10^{9} mL^{-1}
K_{P}	4×10^{11} mL^{-1}
ψ_{MAX}	0.035 min^{-1}
γ_{MAX}	3×10^{-10} mL min^{-1}
β_{MAX}	3×10^{-11} mL min^{-1}
$\psi_{\mathrm{P\,MAX}}$	6 min^{-1}
λ_{T}	$1/90$ min^{-1}
λ_{X}	$1/30$ min^{-1}
λ_{N}	$1/30$ min^{-1}
P_{ψ}	0.6
P_{γ}	0.1

In terms of the plausibility of the maximum conjugation rate, the estimated value can be compared with previous reported values on two levels. On population level, the best fit value $\gamma_{\mathrm{MAX}} = 3 \times 10^{-10}$ mL min^{-1}

is not only in agreement with previous estimates [92, 100–102] of the bulk conjugation rates found through functional transconjugant enumeration (10^{-8} to 10^{-15} mL min^{-1}), but also it fits experiments over a broad range of F+ to F- ratios (from 1:1 to 1:10^3). On individual donor level, γ_{MAX} has to be converted to the maximum conjugation rate per donor first. In this experiment, donor concentrations vary from 10^6 to 10^9 mL^{-1}, hence the corresponding conjugation rate per donor varies from 0.5×10^{-3} to 0.5 min^{-1}. The upper limit is consistent with previous estimates of 0.15 min^{-1} [74] and 0.25 min^{-1} [103].

In terms of the reliability of the maximum conjugation rate, the estimated value leads to simulations that agree well with the growth data generated from a large range of initial donor to recipient concentration ratios.

This plausible and reliable estimated value also has one obvious advantage compared to the estimates through other methods like selective culturing or fluorescence labeling. Estimates from these other methods encompass two distinctive steps: the actual conjugation step that starts from donor recipient encountering and ends with transfer of plasmid; the functional transconjugants formation step that requires recipient to transcribe and translate the antibiotic resistance gene or fluorescence protein encoding gene from newly acquired plasmid. As one can see already, the second step causes these estimated values to depend on the choice of selective or fluorescence markers. Because this measurement bypasses the the additional mechanistic step of functional transconjugants formation, the estimated maximum conjugation value more accurately represents the fundamental process of conjugation—the transfer of genetic information through the medium of plasmid.

To understand the physical significance of γ_{MAX}, notice the term representing the number of conjugations per unit time per unit volume $\gamma(r)n_{\mathrm{D}}n_{\mathrm{R}}$ in Equations (2.6) to (2.9), is analogous to the number of encounters per unit time per unit volume for two kinds of spherical particles in liquids. The encounter rate

of two kinds of molecules A and B of identical radius due to diffusion is [103]

$$\frac{8k_{\mathrm{B}}T_{\mathrm{K}}}{3\eta}n_{\mathrm{A}}n_{\mathrm{B}} = sn_{\mathrm{A}}n_{\mathrm{B}} \tag{2.30}$$

where k_{B} is the Boltzmann constant ($1.38 \times 10^{-23}\,\mathrm{J\,K^{-1}}$), T_{K} is temperature ($310\,\mathrm{K}\,(37\,^{\circ}\mathrm{C})$), η is viscosity of the liquid ($1\,\mathrm{mPa\,s}$), n_{A} and n_{B} are the concentrations of particles A and B respectively. Using these values, I found the search rate to be

$$s = \frac{8 \times 1.38 \times 10^{-23} \times 310}{3 \times 1 \times 10^{-3}} = 1.14 \times 10^{-17}\,\mathrm{m^3 s^{-1}} = 6.84 \times 10^{-10}\,\mathrm{mL\,min^{-1}} \tag{2.31}$$

which is the same order of magnitude as the value of the maximum conjugation rate $\gamma_{\mathrm{MAX}} = 3 \times 10^{-10}\,\mathrm{mL\,min^{-1}}$. This suggests that most encounters result in plasmid transfer: conjugation is operating at an efficiency level close to physical limits.

In terms of the phage results, the 40 % reduction in growth rate is in good agreement with a recent works [99, 104]. I found the maximum phage production rate of an infected cell of $\psi_{\mathrm{P\,MAX}} = 6\,\mathrm{min^{-1}}$ is also in agreement with the recently reported values of $1\,\mathrm{min^{-1}}$ [99] and the historical work reporting $\sim 2\,\mathrm{min^{-1}}$ [105, 106].

Finally, to put the maximum phage infection rate $\beta_{\mathrm{MAX}} = 3 \times 10^{-11}\,\mathrm{mL\,min^{-1}}$ in perspective, note the order of magnitude is very similar to the encounter rate and γ_{MAX} discussed above. To understand the competition between conjugation and phage infection (F- cell and M13 phage compete for the pili of the F+ cell), I can compare the conjugation frequency to phage infection frequency at the onset of mixing. In our model, the encounter of donor F+ and recipient F- cells results in the conjugation frequency of $\gamma(r)n_{\mathrm{D}}n_{\mathrm{R}}$, whereas the encounter of donor F+ cells and M13 phage leads to the infection frequency of $\beta(r)n_{\mathrm{D}}n_{\mathrm{P}}$. The

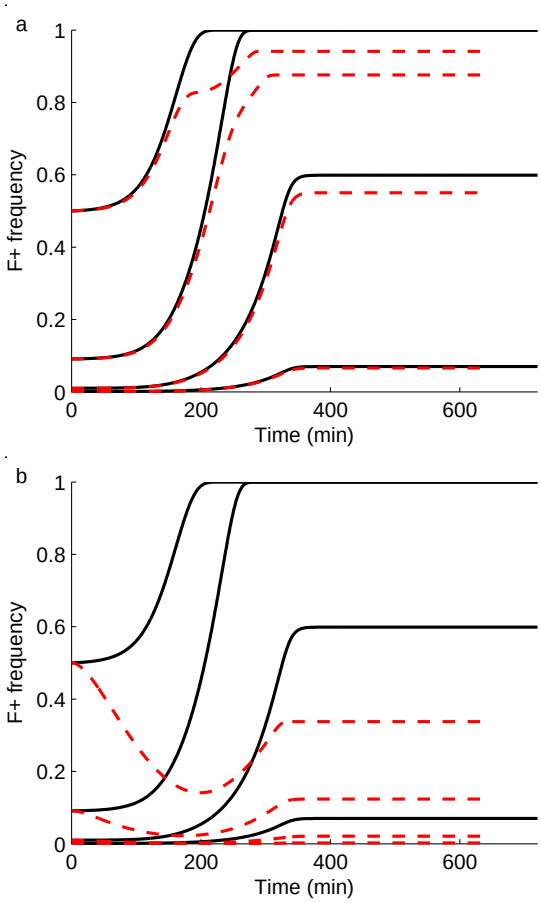

Figure 2.8: Black solid lines represent F+ cell frequency during conjugation without phage, and red dashed lines represent F+ cell frequency during conjugation with phage infection. Each pair of lines from top to bottom represent a different inoculation ratio of F+ to F- cells: 1:1, 1:10, $1{:}10^2$, and $1{:}10^3$. The difference between these two represents the effect of inhibition of conjugation due to M13 phage (a) Within the regime of inoculum concentrations of F- cells and M13 phage $\sim$ 0.1, the effect of phage infection has a small but observable effect on conjugation dynamics.(b) When the inoculum concentrations of F- cells and M13 phage $\sim$ 0.001, the final F+ cell frequencies see a sharp decrease with M13 phage. For ratios of F+ to F- cells $1{:}10^2$ and $1{:}10^3$, conjugation is totally inhibited. Parameters used in the simulation are the same as Table 2.3. Initial conditions for the four different starting ratios: F+ cells 0.5×10^6, 10^5, 10^4 and 10^3; F- cells 0.5×10^6, 10^6, 10^6 and 10^6; M13 (a)1.5×10^7 (b)1.5×10^9

ratio of conjugation frequency to phage infection frequency is

$$\frac{\gamma(r)n_D n_R}{\beta(r)n_D n_P} = \frac{\gamma_{MAX} n_R}{\beta_{MAX} n_P} \tag{2.32}$$

From estimated values of parameters, $\gamma_{MAX}/\beta_{MAX} = 10$, with a population difference of F- cells to M13 phage of $n_R/n_P \sim 0.1$ upon inoculation. Hence a F+ cell has a similar probability of encountering a F- and conjugating as being infected by a M13 phage. This contributes to the small difference of the trends of F+ cells between conditions of without M13 phage (Figure 2.5b) and with M13 phage (Figure 2.7b). Comparing the simulation results of the F+ cell frequency versus time for both conditions (Figure 2.8a), it also confirms within the regime of my experiment, M13 phage only has a small effect on conjugation. Equation (2.19) predicts that the use of phage to regulate the conjugative spread of antibiotic resistance markers requires a regime where $n_R \ll n_P$ by several orders of magnitude. Recent kinetic studies [99] indeed showed $n_R/n_P \sim 0.001$ is sufficient for total inhibition of conjugation, and simulation using this condition yields the same conclusion (Figure 2.8b).

3

Mutators

The majority of spontaneous mutations are neutral or deleterious, and only a small number of them are beneficial. Organisms have evolved lower spontaneous mutation rates through DNA proofreading and repairing system that ensures the fidelity of DNA replication. Increasing the spontaneous mutation rate of a cell should in general decrease its fitness due to accumulation of deleterious mutations.

The mutator phenotype exhibits elevated spontaneous mutation rate, and the accumulated deleterious mutations will in turn, lower mutator phenotype's fitness comparing to its wild-type counterpart. Thus, in theory, a mutator phenotype should be scarce in nature, if it even exists. Contrary to this plausible rea-

soning, the mutator phenotype has been observed in natural th*Escherichia coli* (*E. coli*) and other microbial populations [52, 60–62, 107, 108]. And the frequency of the mutator phenotype is even higher among isolates from clinical environment [63, 109, 110].

One of the major causes of mutator phenotype, especially among clinical isolates, results from the genetic alternation of DNA mismatch repair system (MMR). MMR related genes (*mutS*, *mutL*, *mutH*, *uvrD* and *dam*) are responsible for proofreading and repairing base substitution mismatches and insertion-deletion mismatches during DNA replication and recombination [111, 112]. Inactivation of any of these MMR related genes converts wild-type into mutator phenotype with strong mutator effect. Mutator phenotypic cells with defects in MMR exhibit mutation rate increasing 100- to 1000-fold comparing to wild-type, and produce G:C $\rightarrow$ A:T and A:T $\rightarrow$ G:C transversions and 1–4 bp frameshift [113, 114].

This chapter uses the same novel quantitative PCR assay developed in Chapter 2 to investigate under what circumstances mutator phenotype can achieve fixation when competing with wild-type phenotype.

An *E. coli* strain with *mutL* deletion is chosen as the mutator phenotype. MutL protein has been shown to be an ATPase, and together with mismatch recognition protein MutS protein, they play essential roles in initiating repair mechanisms [114, 115]. By deleting MutL protein's two amino acids, which lie in the region that forms the lid of the ATP-binding pocket, a study has shown that mutation rate increases more than two orders of magnitude in *Salmonella typhimurium*; and completely deleting *mutL* gene, the mutation rate is further increased [116]. Another study using *E. coli mutL* deletion strain also reported more than 100-fold increase of mutation rate using mutation-accumulation (MA) strategy, which ensures the occurrence of mutations devoid of selective pressure[117]. In contrast, introducing high copy numbers of *mutL* gene can yield an anti-mutator phenotype with more than twofold decrease in mutation rate compared to wild-type [118].

Streptomycin is chosen as the antibiotic selective pressure factor for the competition experiment. Streptomycin is an aminoglycoside antibiotic that affects the accuracy of translation through tight interaction with the 30S ribosomal subunit [119, 120]. Several studies have established that exposing to streptomycin

increases the mutation rate of *E. coli* cells [121, 122], and one study even shows that streptomycin can further increase the already elevated mutation rate of *mutL* mutants [121].

I will start by investigating the growth behaviors of wild-type and mutators when they are grown in isolation. Then the effect of adding low concentration streptomycin (see Section 3.1.2 for details regarding the concentration) as selective pressure will also be evaluated.

Then I will compete wild-type with mutators through serial passage with different initial population compositions and different degrees of selective pressure. The selective advantage confirmed by antibiotic resistance mutation will also be quantified through analysis of competition results.

Finally I will present a simple theoretical model of the wild-type/mutator competition simulation, and study how mutators influence the adaption process for asexual population in a new environment by examining the effects of population size, selective coefficient and strength of mutator effect.

3.1 Materials and Methods

3.1.1 Strains

E. coli strain BW25113 (F-, *Δ(araD-araB)567, ΔlacZ4787(*::rrnB-3*)*, λ-, *rph-1, Δ(rhaD-rhaB)568, hsdR514*) and JW4128-1 (F-, *Δ(araD-araB)567, ΔlacZ4787(*::rrnB-3*)*, λ-, *rph-1, Δ(rhaD-rhaB)568, ΔmutL720::kan, hsdR514*) were acquired from the Yale Coli Genetic Stock Center. Both the parent strain BW25113 and its *mutL* knockout strain JW4128-1 came from the Keio Collection of single gene knockouts [123].

3.1.2 Growth Assays

All growth assays were carried out using Davis Minimal Broth supplemented with dextrose with a concentration of 1000 mg L^{-1} (DM1000). 5X Supplement EZ (AA) from EZ Rich Defined Medium [124] was also added to the broth at 1:4 ratio as amino acids supplement (DM1000+AA). When selective pres-

sure is required, streptomycin sulfate (Fisher Scientific, Hampton, NH) was added into the broth to a final concentration of 2 μg mL^{-1} (See Section 3.4 for details about the streptomycin concentration choice).

For separate growth experiments, overnight cultures of wild-type and mutators in DM1000+AA were used as initial inoculum, and 2 μL of each strain was inoculated into 148 μL DM1000+AA medium and DM1000+AA supplemented with 2 μg mL^{-1} streptomycin. The growth experiments were carried out on 96 well flat bottom Corning Costar culture plates(Corning Incorporated, Corning, NY). Every strain/medium combination (wild-type without streptomycin, mutator without streptomycin, wild-type with streptomycin and mutator with streptomycin) was repeated in 20 wells (each well represents one collecting time point). To prevent evaporation and cross contamination, plates were covered with breathe easier membranes (USA Scientific, Ocala, FL) before putting the plate lids on. The plates were incubated on a plate shaker at 1350 rpm at 37 °C. Every 30 min, 5 μL of cells from every strain/medium combination was collected from one of the 20 repeated wells into 95 μL Milli-Q water and lysed on a dry bath at 95 °C for 5 min, and stored at −20 °C until used as template for qPCR assay.

Three different conditions of selective pressure was tested during competition experiments: i) DM1000+AA only, ii) daily alternations between DM1000+AA and DM1000+AA supplemented with 2 μg mL^{-1} streptomycin, and iii) DM1000+AA supplemented with 2 μg mL^{-1} streptomycin only.

Similar to separate growth experiments, competition experiments also used overnight cultures in DM1000+AA as inoculum. Different ratios of wild-type/mutator (10^2:1, 10^1:1, 1:1, 1:10^1, 1:10^2) overnight cultures were mixed first in a 1.7 mL tube, and 2 μL of each mixture was inoculated into 148 μL fresh medium into 96 well flat bottom Corning Costar culture plates. After every 24 h, 2 μL of culture from each well was transferred into a new well with 148 μL fresh medium. After making the transfer, another 5 μL of culture from each well was collected and diluted with 95 μL Milli-Q water and incubated on a dry bath at 95 °C for 5 min, and stored at −20 °C until used as template for qPCR assay.

3.1.3 Quantitative PCR Assay

For the quantitative PCR (qPCR) assay, a 10 µL qPCR reaction mixture was used, and it contained the following components: 200 µM of each dNTP, 0.4U (per 10 µL volume) Roche FastStart Taq DNA polymerase (Roche Diagnostics), 1X Roche FastStart Buffer (Roche Diagnostics), 0.4 µM of forward and reverse primers (see Table 3.1 for primer details), 2 µM SYTO 9 green fluorescent nucleic acid stain (Invitrogen) and 2 µL of template.

All reactions were performed in a CFX Connect Real-Time PCR Detection System (Bio-Rad Laboratories), in 96 well, clear bottom, hard shell, skirted assay plates (Bio-Rad Laboratories) with Microseal B sealing tape (Bio-Rad Laboratories). The instrument filter setting was set for FAM. Primers used in mutator study are summarized in Table 3.1. Thermal cycles used are following: one cycle of 95 °C for 4 min, followed by 35 cycles of 95 °C for 30 s, 55 °C for 30 s, plate read, and 72 °C for 20 s.

Table 3.1: Primers used in mutator study

Primers	$5' \rightarrow 3'$
tolC Forward	CGACAAACCACAGCCGGTTA
tolC Reverse	CAGCGAGAAGCTCAGGCCA
mutL Forward	CACCCCGCCAAACACGAA
mutL Reverse	GGACGACTGCCTGATGCT

Both *tolC* and *mutL* are chromosomal loci that are present in BW25113 (wild-type strain), however *mutL* is not present in JW4128-1 (*mutL* deletion mutator strain). The C_t values were converted into cell concentrations by using standard curve method. Standard curves of both tolC and mutL primers are generated by using the same templates of 10-fold serial dilutions of overnight BW25113 culture with known concentration ranging from 4×10^6 to 4×10^9 mL^{-1}. By relying on the linear regression equation of the known concentration and C_t values of these serial dilutions, one can interpolate the unknown template's concentration. Because for BW25113 strain, the ratio of *tolC* to *mutL* is 1:1, by using the same templates for both

tolC and mutL primers, we can correct for any efficiency difference between them.

3.2 Results

3.2.1 Separate Growth

Wild-type and mutator cells should both follow logistic growth (growth curves are shown in Figure 3.1 right column) if grown in isolation:

$$\frac{dn}{dt} = rn(1 - \frac{n}{K}) \tag{3.1}$$

where n is the cell density, r is the growth rate, and K is the cell carrying capacity. Equation (3.1) can be rearranged with all n related terms on the left-hand side, while leaving other terms on the right-hand side:

$$\frac{dn}{n(n-K)} = \frac{r}{K}dt \tag{3.2}$$

Integrating both sides yields the following linear relation:

$$\ln \frac{K-n}{n} = -rt + C \tag{3.3}$$

where C is a constant.

K can be determined by averaging the separate growth experiments' saturation phase data (data points after 420 min in Figure 3.1 left column). The results are summarized in Table 3.2 with standard deviation showing as uncertainty inside parentheses.

After obtaining K, the linear regression model specified in Equation (3.3) can be fitted with the separate growth experiment's exponential phase data (data points before 270 min in Figure 3.1 left column). The absolute value of the regression slope of log-population size versus time corresponds to the growth rate r.

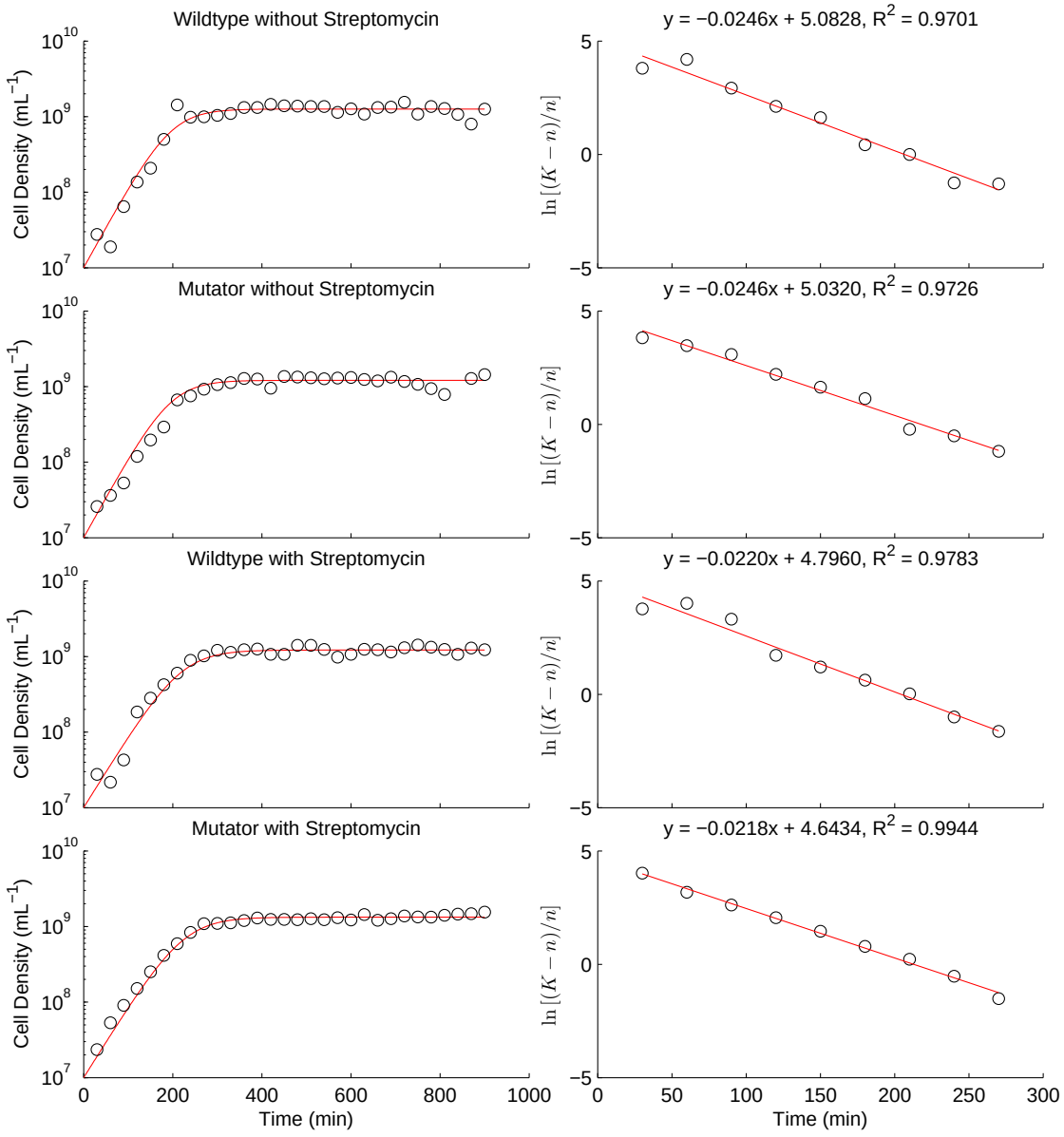

Figure 3.1: Left column: time series plots of wild-type and *mutL* deletion mutators grow separately without streptomycin and with low concentration of 2 μg mL^{-1} streptomycin as antibiotic selective pressure. Circle represents growth data point measured from qPCR using tolC primers, and red line represents the fitted curve. Right column: corresponding linear regression model best-fit of exponential growth phase. The slope corresponds to growth rate. Circle represents the transformed growth data point (see Equation (3.3) for details), and red line represents the bet-fit line

The best-fit lines and linear regression fitting results are summarized in Figure 3.1 right column.

One can clearly see, as expected, both wild-type and *mutL* deletion mutator cells exhibit decreased growth rate when 2 $\mu g\,mL^{-1}$ streptomycin is added: wild-type growth rate decreases from 0.0246 min^{-1} to 0.0220 min^{-1}; mutator growth rate decreases from 0.0246 min^{-1} to 0.0218 min^{-1}. But surprisingly, the growth rates of wild-type and mutator cells are almost identical with or without streptomycin. This means the *mutL* deletion within the mutator ancestor strain doesn't cause either fitness advantage or disadvantage compared to the wild-type ancestor strain when grown in DM1000+AA growth medium with or without streptomycin. And it is because of this trait, the *mutL* deletion mutator is chosen among several different mutators for competition experiment. The fitness similarities between these two strains imply during competition growth experiments, the fitness increase should come from beneficial mutations acquired during competition.

Table 3.2: Parameter values used in separate growth fitting

Physical Quantity	wild-type without Streptomycin	Mutator without Streptomycin	wild-type with Streptomycin	Mutator with Streptomycin
r	0.0246 min^{-1}	0.0246 min^{-1}	0.0220 min^{-1}	0.0218 min^{-1}
K	$1.26(18)\times10^9$ mL^{-1}	$1.21(18)\times10^9$ mL^{-1}	$1.22(14)\times10^9$ mL^{-1}	$1.33(11)\times10^9$ mL^{-1}

3.2.2 Competition Growth

Figure 3.2 shows *mutL* deletion mutator and wild-type competition results after five days grouped by selective pressure conditions.

Figure 3.2a shows competition results with no added antibiotic selective pressure. One can clearly notice the competition results depend on the starting wild-type:mutator ratio (frequency dependent). When

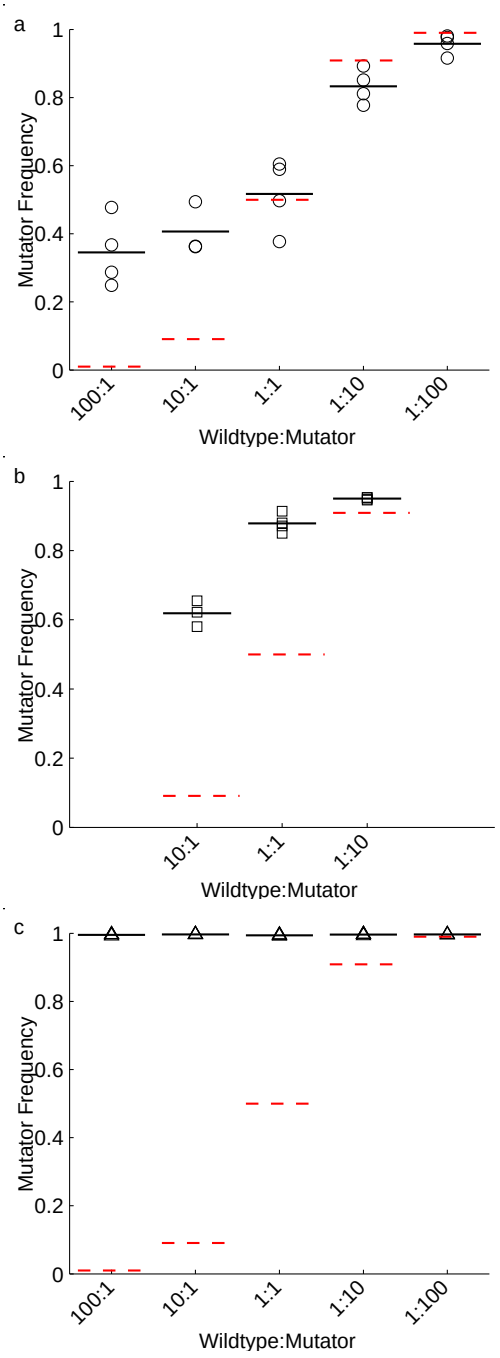

Figure 3.2: Mutator frequencies after day 5 of competition between *mutL* deletion mutator and wild-type in DM1000+AA medium with (a)no added streptomycin (circle), (b)no and 2 µg mL^{-1} streptomycin alternating everyday (square) and (b)2 µg mL^{-1} streptomycin (triangle). x-axis specifies the starting wild-type:mutator ratio at day 0, and dotted red line denotes corresponding starting mutator frequency. Black solid line denotes the average mutator frequencies of four duplicates (symbol) after day 5

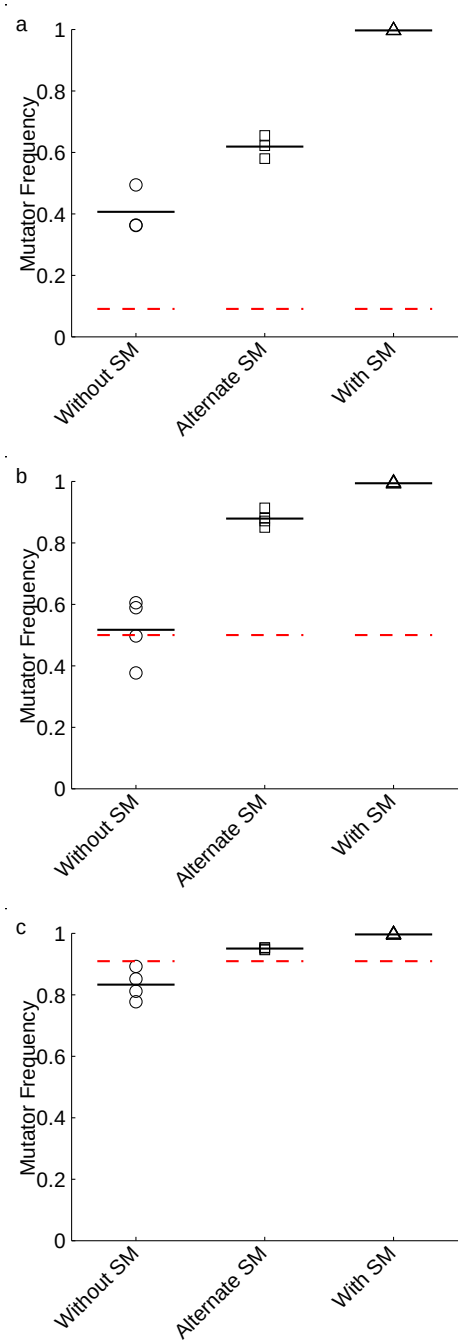

Figure 3.3: Mutator frequencies after day 5 of competition between *mutL* deletion mutator and wild-type in DM1000+AA medium with no added streptomycin (SM) (circle), 2 μg mL^{-1} streptomycin (square) and no and 2 μg mL^{-1} streptomycin alternating everyday (triangle) with starting ratio of wild-type:mutator (a) 10:1, (b) 1:1 and (c) 1:10. x-axis specifies the selective pressure condition. Dotted red line denotes starting mutator frequency at day 0, and black solid line denotes the average mutator frequencies of four duplicates (symbol) after day 5

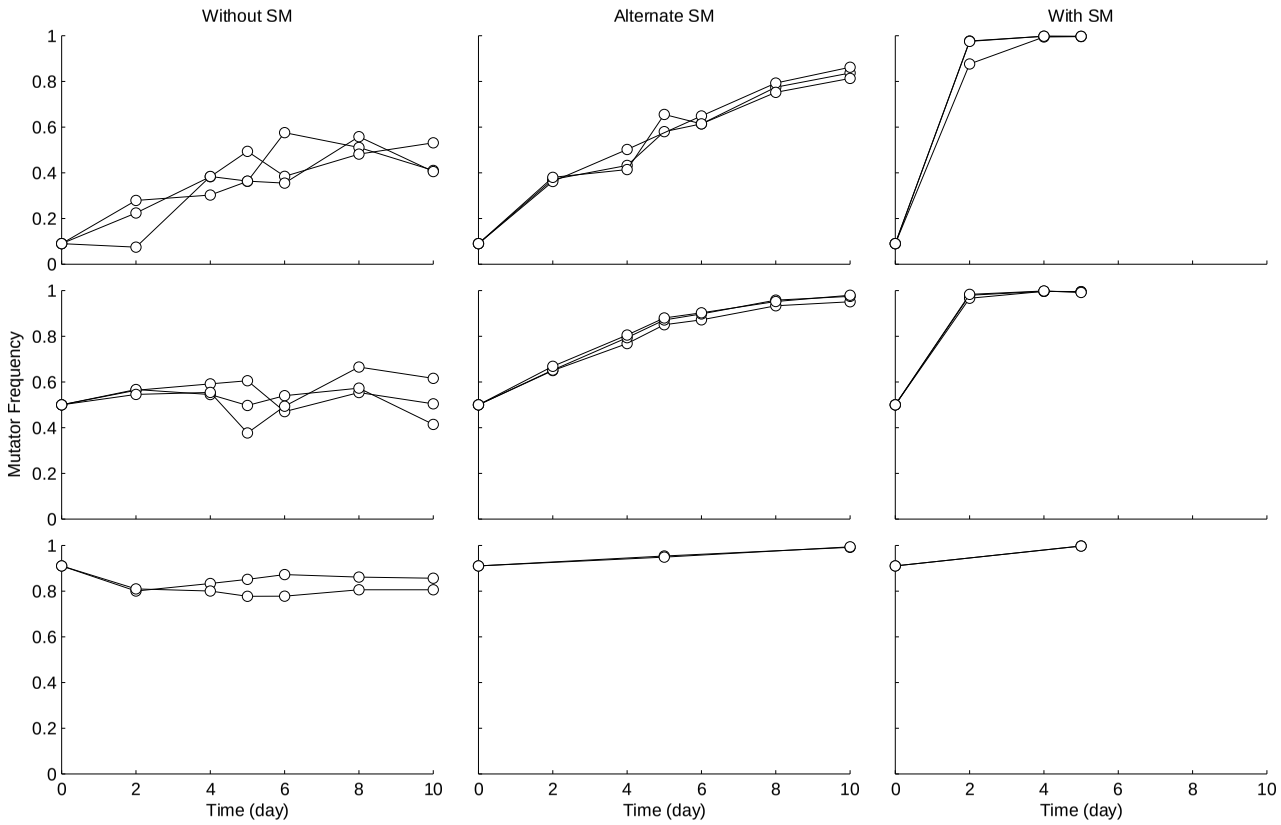

Figure 3.4: Mutator frequency time series of competition between *mutL* deletion mutator and wild-type in DM1000+AA medium with no added streptomycin (SM) (first column), no and 2 $\mu g\,mL^{-1}$ streptomycin alternating everyday (second column) 2 $\mu g\,mL^{-1}$ streptomycin (third column) with starting ratio of wild-type:mutator 10:1 (first row), 1:1 (second row) and 1:10 (third row) at day 0. Each group of circles connected by lines represents one competition population mixture, and groups within each sub-figures represent competition population mixture duplicates

starting with majority of wild-type cells (wild-type:mutator 100:1 and 10:1), at the end of day 5, wild-type cells still outnumber mutator cells (wild-type:mutator ∼3:2). But when starting with majority of mutator cells (wild-type:mutator 1:10 and 1:100), at the end of day 5, mutator cells still constitute a very large portion of the population (wild-type:mutator *sim*1:9). When starting with comparable amount of wild-type and mutator cells (wild-type:mutator 1:1), at the end of day 5, the competition outcome is stochastic but the winning margin is always small, with wild-type or mutator represent between 40–60 % of the total population. To summarize competition without selective pressure, neither wild-type nor mutator can drive the other to extinction but approaches equilibrium determined by the starting ratio.

Figure 3.2b shows competition results with alternating everyday between no antibiotics and 2 $\mu g\,mL^{-1}$ added streptomycin. Under this condition, at the end of day 5, mutator cells always outperform wild-type under all three starting ratios tested (wild-type:mutator 10:1, 1:1 and 1:10). This suggests that under selective condition, mutator cells confirm a higher fitness due to acquired beneficial mutations.

Figure 3.2c shows a clearer picture of mutator cells' fitness advantage through elevated mutation rate when streptomycin is present at all time. The five different starting ratios (wild-type:mutator 100:1, 10:1, 1:1, 1:10 and 1:100) all share the same outcome: at the end of day 5, mutator cells drive the wild-type almost to extinction with final population almost 100 % mutator cells.

Figure 3.3 re-plots Figure 3.2 but grouped by starting wild-type:mutator ratios (10:1, 1:1 and 1:10). All three ratios exhibit the same trend: as the level of selective pressure increases (without streptomycin, alternate streptomycin, with streptomycin), mutator cells' final frequency also increases.

In order to see the dynamics of the competition between wild-type and mutator cells, selected time series of mutator frequencies from day 0 to day 10 are shown in Figure 3.4.

In the absence of streptomycin as selective pressure, neither wild-type nor mutator can drive the other to extinction. After 10 days of competition, wild-type and mutator reached equilibrium with a relatively fixed ratio (Figure 3.4 first column). But when streptomycin is added every other day, mutator starts to drive wild-type to extinction by acquiring beneficial mutations faster through elevated mutation rate (Figure 3.4

second column). When streptomycin is present in the media constantly, the rate of the whole population converging to mutator increases (Figure 3.4 third column).

From a more quantitative view point, Figure 3.4 can be used to estimate fitness effects of mutations by relating to the selection coefficient s. Consider an asexual population consisting of mutator and wild-type cells with frequencies p and $q = 1 - p$. The selection coefficient s of this continuous growth culture can be defined as:

$$\begin{aligned} s &= \frac{d}{dt} \ln \frac{p}{q} \\ &= \frac{d}{dt} \ln \frac{p}{1-p} \end{aligned} \tag{3.4}$$

[125], with the units of time^{-1}. If $s > 0$, mutator cells have fitness advantage comparing to wild-type. If $s < 0$, mutator cells have fitness disadvantage comparing to wild-type.

The definition of selection coefficient s of continuous growth from Equation (3.4) can also be formulated equivalently for discrete non-overlapping generations:

$$s_T = \ln \left(\frac{p'/(1-p')}{p/(1-p)} \right) \tag{3.5}$$

[126], with primes denotes the values in the next generation. Here s_T represents the selection coefficient is evaluated over generation time, and therefore has the units of generation^{-1}.

For the serial passage competition assay used in this experiment, the number of generations T between each passage can be estimated using the dilution factor $D = 75$:

$$T = \log_2 D = \log_2 75 \tag{3.6}$$

And the ratio of mutator and wild-type cells at the end of day k-1 before dilution is the same as the ratio at

the beginning of day k:

$$p_{\text{day k-1, f}}/(1 - p_{\text{day k-1, f}}) = p_{\text{day k, i}}/(1 - p_{\text{day k, i}}) \tag{3.7}$$

with subscripts i and f denote the initial and finial states of each passage. Therefore, the selection coefficient evaluated over one passage is:

$$\begin{aligned} s_{\text{T}} &= \frac{1}{T} \ln \left(\frac{p_{\text{day k, f}}/(1 - p_{\text{day k, f}})}{p_{\text{day k, i}}/(1 - p_{\text{day k, i}})} \right) \\ s_{\text{T}} &= \frac{1}{T} \ln \left(\frac{p_{\text{day k, f}}/(1 - p_{\text{day k, f}})}{p_{\text{day k-1, f}}/(1 - p_{\text{day k-1, f}})} \right) \end{aligned} \tag{3.8}$$

and the subscript f can be omitted from now on.

Because Figure 3.4 is sampled at a rate of one datum point per two days, the estimation of selection coefficient calculated from it also has to be modified as following:

$$s_{\text{T}} = \frac{1}{2T} \ln \left(\frac{p_{\text{day k}}/(1 - p_{\text{day k}})}{p_{\text{day k-2}}/(1 - p_{\text{day k-2}})} \right) \tag{3.9}$$

In the absence of streptomycin as selective pressure, the selection coefficient gradually converges to zero, which signals the ratio between mutator and wild-type cells approaching equilibrium (Figure 3.5 first column). After equilibrium is reached, the mutator frequency should stay constant. When streptomycin is added every other day, the selection coefficient stays around 0.05, which roughly represents mutator cells have about 5 % fitness advantage per generation compared to wild-type under this condition (Figure 3.5 second column). When streptomycin is present at all times, the selection coefficients of all cell cultures have a even more sizable increase with an value between 0.15 to 0.20, which represents about 15 to 20 % mutator fitness advantage per generation compared to wild-type in this situation (Figure 3.5 third column).

Recall the growth rates of separate growth: both wild-type and mutator grow at 0.0246 min^{-1} without streptomycin; when streptomycin is present, they grow at 0.0220 min^{-1} and 0.0218 min^{-1} respectively. This

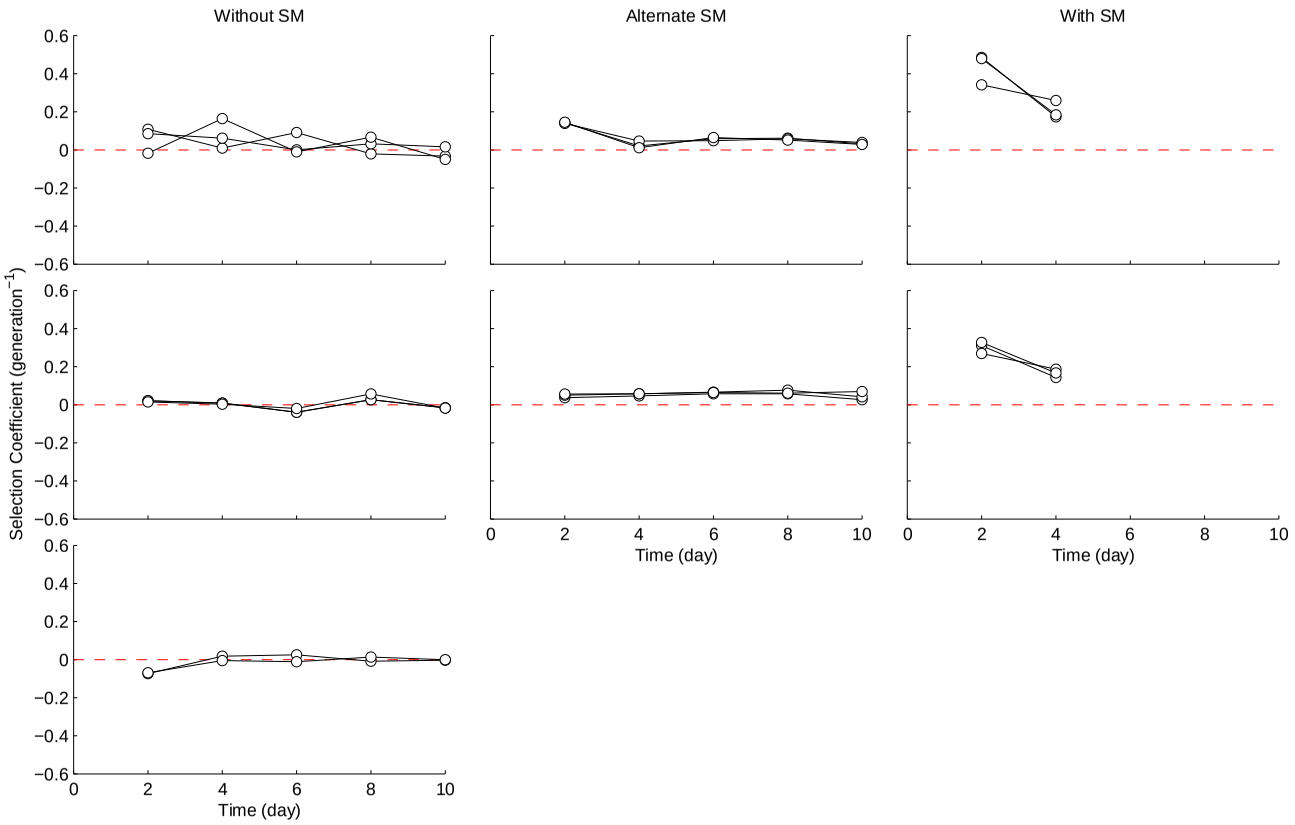

Figure 3.5: Selection coefficient estimation time series of competition between *mutL* deletion mutator and wild-type in DM1000+AA medium with no added streptomycin (SM) (first column), no and 2 μg mL^{-1} streptomycin alternating everyday (second column) 2 μg mL^{-1} streptomycin (third column) with starting ratio of wild-type:mutator 10:1 (first row), 1:1 (second row) and 1:10 (third row) at day 0. Each group of circles connected by lines represents one competition population mixture, and groups within each sub-figures represent competition population mixture duplicates. Red dashed line shows when selection coefficient is zero.

means when growing at the presence of streptomycin, if the cell picks up the beneficial resistance mutation that offsets the growth penalty due to streptomycin, the cell will have an increase of growth rate. And the selective coefficient of streptomycin resistant type of cell compared to streptomycin non-resistant one can be estimated as

$$\begin{aligned} s_{\mathrm{T}} &= (r_{\text{Resistant}} - r_{\text{Non-resistant}})T \\ &= \frac{r_{\text{Resistant}} - r_{\text{Non-resistant}}}{r_{\text{Non-resistant}}} \ln 2 \end{aligned} \tag{3.10}$$

[126], where $T = \ln 2 / r_{\text{Non-resistant}}$ is the generation time of streptomycin non-resistant cells, and it has units of generation^{-1} as in Equation (3.9). The selective coefficient confirmed by acquiring a streptomycin resistance mutation can be calculated for wild-type and mutators:

$$s_{\mathrm{T,WR,W}} = \frac{r_{\mathrm{WR}} - r_{\mathrm{W}}}{r_{\mathrm{W}}} \ln 2 = \frac{0.0246 - 0.0220}{0.0220} \ln 2 = 0.08 \tag{3.11}$$

$$s_{\mathrm{T,MR,M}} = \frac{r_{\mathrm{MR}} - r_{\mathrm{M}}}{r_{\mathrm{M}}} \ln 2 = \frac{0.0246 - 0.0218}{0.0218} \ln 2 = 0.09 \tag{3.12}$$

where the subscripts in $s_{\mathrm{T,WR,W}}$ denotes the selective coefficient between resistant wild-type (WR) and wild-type(W) measured in terms of wild-type(W) generation time. And similarly, the subscripts in $s_{\mathrm{T,MR,M}}$ represents the selective coefficient between resistant mutators (MR) and mutators(M) measured in terms of mutator(M) generation time. Notice these estimated selective coefficient values are smaller than 0.15 to 0.20, the values estimated from competition experiment under streptomycin condition. See Discussions for possible reasons behind this discrepancy.

3.3 Simulation

The aim of this section is to quantify the effects of important parameters for the competition experiment between mutator and wild-type cells under selective pressure. By modifying a theoretical model for evolution in single-peak adaptive landscape[56], I will examine the influence of mutator phenotype on the adaptation process in a finite asexual population.

3.3.1 Simulation Algorithm

The population starts with only wild-type and mutator cells without antibiotic resistance, and then selective pressure (streptomycin) is added. When beneficial mutation (streptomycin resistance) arises, it enables its bearing cell selective advantage s. From generation t to generation $t+1$, the population undergoes three processes: replication-selection, mutation and random sampling. The simulation tracks the number of individuals of the four different genotypes present within the population: Wild-type n_{W}, Wild-type Resistant to streptomycin n_{WR}, Mutator n_{M} and Mutator Resistant to streptomycin n_{MR}. Figure 3.6 shows the schematic of the simulation algorithm, and the details of each process are described below.

Replication-Selection Process: At generation t, the number of individuals of genotype starts with n_i $(i = \mathrm{W}, \mathrm{WR}, \mathrm{M}, \mathrm{MR})$. After replication-selection process, the number of individuals of genotype n_i' is randomly drawn from a Poisson distribution with expected value of

$$\mathrm{E}[n_i'] = n_i(1 + s_i) \tag{3.13}$$

where s_i is the selective coefficient. Wild-type and mutator before acquiring streptomycin resistance both have the same fitness of 1, therefore $s_{\mathrm{W}} = s_{\mathrm{M}} = 0$. Streptomycin resistance mutation increases their fitness

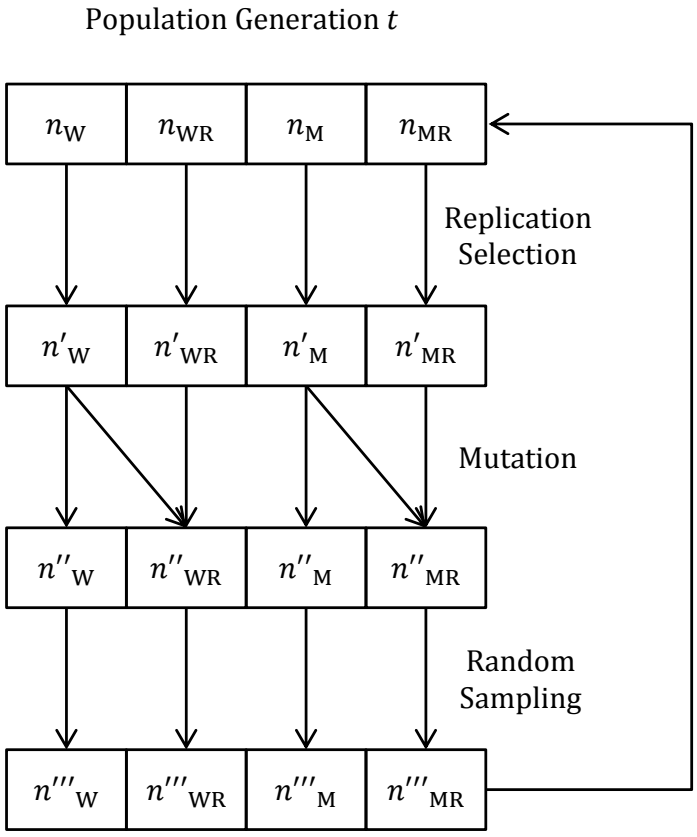

Figure 3.6: Schematic of the simulation algorithm of competition between mutator and wild-type cells under selective pressure. The population consists of four genotypes: Wild-type (W), Wild-type Resistant to streptomycin (WR), Mutator (M) and Mutator Resistant to streptomycin (MR). From generation t to generation $t+1$, each genotype undergoes replication-selection, mutation and random sampling process Figure 3.5. See details of each process in text Section 3.3.1

by the same selective coefficient $s_{WR} = s_{MR} = s$. Specifically, apply Equation (3.13) to each genotype:

$$\mathrm{E}[n'_{W}] = n_{W} \tag{3.14a}$$

$$\mathrm{E}[n'_{WR}] = n_{WR}(1+s) \tag{3.14b}$$

$$\mathrm{E}[n'_{M}] = n_{M} \tag{3.14c}$$

$$\mathrm{E}[n'_{MR}] = n_{MR}(1+s) \tag{3.14d}$$

Mutation Process: The number of individuals of each genotype after mutation n''_i comes from two different sources. Some cell population come from their original type i which do not go through mutation, and the other population come from other type j mutate into type i. The number of individuals of genotype after mutation is also drawn randomly from a Poisson distribution with expected value of

$$\mathrm{E}[n''_i] = n'_i(1-\mu_i) + \sum_{j \neq i} n'_j \mu_{j \to i} \tag{3.15}$$

where μ_i is the mutation rate of type i mutates to other types, and $\mu_{j \to i}$ is the mutation rate of type j mutates to type i. The model here only have two possible mutation paths: wild-type acquires streptomycin resistance through mutation at rate μ, and mutator acquires the same resistance but at an elevated rate $m\mu$. m is the strength of mutator effect, and it describes mutators' fold increase of mutation rate comparing to wild-type. Equation (3.15) can also be simplified for each genotype:

$$\mathrm{E}[n''_{W}] = n'_{W}(1-\mu) - n'_{W}\mu \tag{3.16a}$$

$$\mathrm{E}[n''_{WR}] = n'_{WR} + n'_{W}\mu \tag{3.16b}$$

$$\mathrm{E}[n''_{M}] = n'_{M}(1-m\mu) - n'_{M}m\mu \tag{3.16c}$$

$$\mathrm{E}[n''_{MR}] = n'_{MR} + n'_{M}m\mu \tag{3.16d}$$

Random Sampling Process: The random sampling process is used to model drift as to keep the population size fixed at each generation. Ideally this should be modeled as random sampling of size N, the population carrying capacity, without replacement from the total population after mutation process $\sum_i n_i''$. But for bacteria, N is too large that the simulation time is too long to be practical for following the exact process. Here I make the simplification by following previous two processes of drawing the number of individuals of each phenotype randomly from a Poisson distribution with expected value of

$$\mathrm{E}[n_i'''] = n_i'' \frac{N}{\sum_j n_j''} \tag{3.17}$$

The rationality behind this is to keep the sum of expected individuals of generation $t+1$ equal to the carrying capacity $\sum_i \mathrm{E}[n_i'''] = N$. Equation (3.17) can be written out in details for each genotype:

$$\mathrm{E}[n_{\mathrm{W}}'''] = n_{\mathrm{W}}'' \frac{N}{n_{\mathrm{W}}'' + n_{\mathrm{WR}}'' + n_{\mathrm{M}}'' + n_{\mathrm{MR}}''} \tag{3.18a}$$

$$\mathrm{E}[n_{\mathrm{WR}}'''] = n_{\mathrm{WR}}'' \frac{N}{n_{\mathrm{W}}'' + n_{\mathrm{WR}}'' + n_{\mathrm{M}}'' + n_{\mathrm{MR}}''} \tag{3.18b}$$

$$\mathrm{E}[n_{\mathrm{M}}'''] = n_{\mathrm{M}}'' \frac{N}{n_{\mathrm{W}}'' + n_{\mathrm{WR}}'' + n_{\mathrm{M}}'' + n_{\mathrm{MR}}''} \tag{3.18c}$$

$$\mathrm{E}[n_{\mathrm{MR}}'''] = n_{\mathrm{MR}}'' \frac{N}{n_{\mathrm{W}}'' + n_{\mathrm{WR}}'' + n_{\mathrm{M}}'' + n_{\mathrm{MR}}''} \tag{3.18d}$$

After random sampling process, the number of individuals of each genotype n_i''' is fed back as n_i for next round of simulation. Simulation stops until either mutator or wild-type cells become extinct, it also stops when preset upper-limit of simulation rounds (500 generations) reaches.

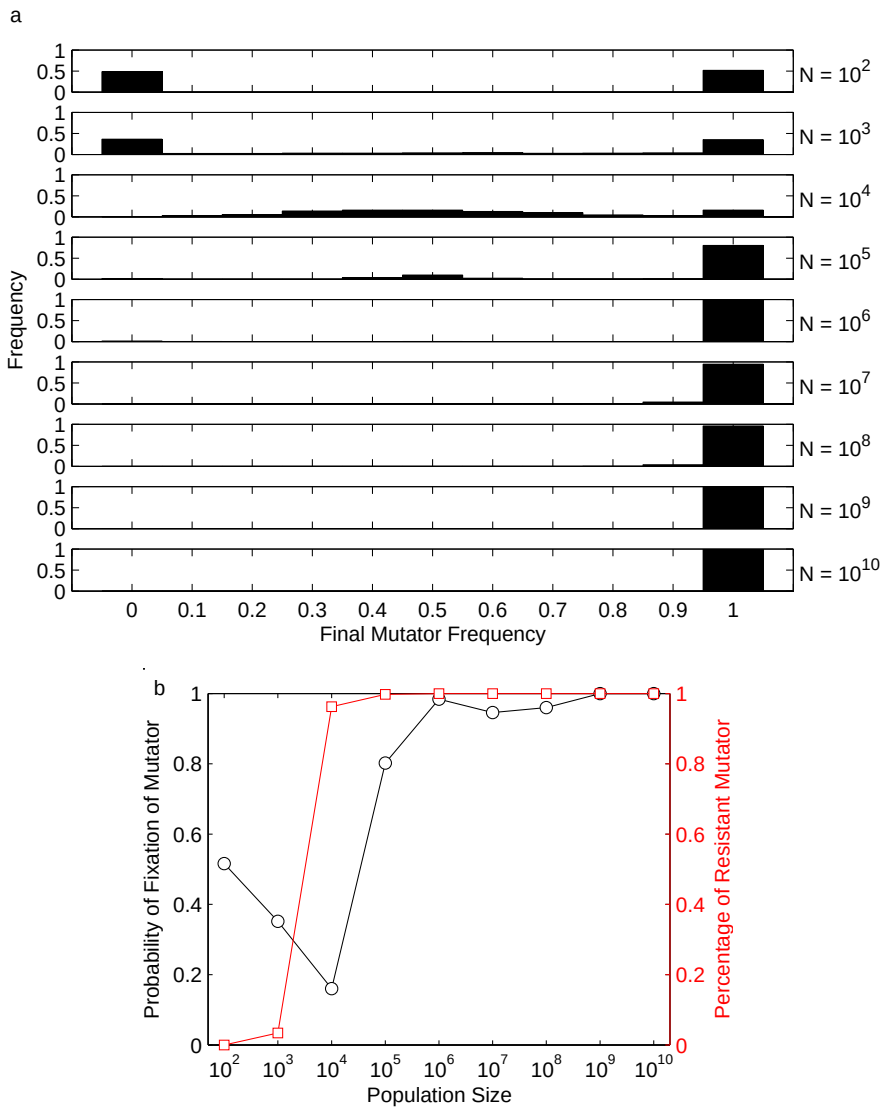

Figure 3.7: (a) Histogram of final mutator frequency of wild-type/mutator competition for different population size. (b) Probability of fixation of mutators (black circle) and percentage of resistant mutators (red square) for different population size. Mutators are fixed when at the end of simulation the mutator consists more than 95 % of the final population. Probability of fixation of mutators are estimated as the percentage of occurrences when mutator cells reach fixation over 500 independent simulations. Percentage of resistant mutators is calculated from simulations when mutators reach fixation. Other parameters used in the simulation: $s = 0.15, \mu = 1 \times 10^{-8}, m = 100$

3.3.2 Simulation Results

Effects of population size N

The effect of population size N on the fixation of mutators are examined by following population size ranging from 10^2 to 10^{10} cells, which consist of half wild-type and half mutators. Mutators are said to be fixed if at the end of 500-generation simulation, mutators reach above 95 % of the total population. Parameter values used in the simulation are chosen as following: selective coefficient $s = 0.15$ is chosen to resemble the values obtained from separate growth experiments from Section 3.2.1; beneficial mutation rate $\mu = 1 \times 10^{-8}$ is the usual estimated values used in similar simulation studies [55, 56, 73]; strength of mutator effect $m = 100$ is chose as the same magnitude of reported value of *mutL* mutator [116, 117].

Figure 3.7a shows a histogram of final mutator frequency for different sizes of population. Final here means either after 500-generation simulation or either mutator or wild-type cells become extinct, whichever of these two happens first. As one can see for small population sizes $N < 10^3$, fixation of either wild-type or mutator cells is usually reached with equal probability (first and last bars of each histogram represents the probability of fixation of wild-type and mutators respectively). When the population size starts to increase $N = 10^4$ the probability of either wild-type and mutator cells becoming fixed decreases, and most of the time, at then end of 500-generation simulation, both genotypes co-exist within the population. But as population size increases beyond $N > 10^5$, the probability of mutators driving wild-type to extinction and becoming fixed approaches 1.

Figure 3.7b summaries the probability of fixation of mutators for different population sizes. It is generated from Figure 3.7a by plotting the last bar (represents the frequency of mutator consisting more than 95 % of the population at the end of simulation) versus population size (black circle). But one has to be careful when interpreting the relation between these two quantities. For small population size cases, the final fixed mutator population is dominated by mutator cells that lack the resistance mutation, and the fixation is due to drift. Whereas for large population sizes, the fixed mutators are dominantly resistant mutator

cells. This can be easily seen by plotting the percentage of resistant mutators for the cases when mutator cells become fixed (red square). As the population size increases, the percentage of resistant mutators also increases, but not necessarily, the probability of fixation of mutators.

Effects of selective coefficient s and strength of mutator effect m

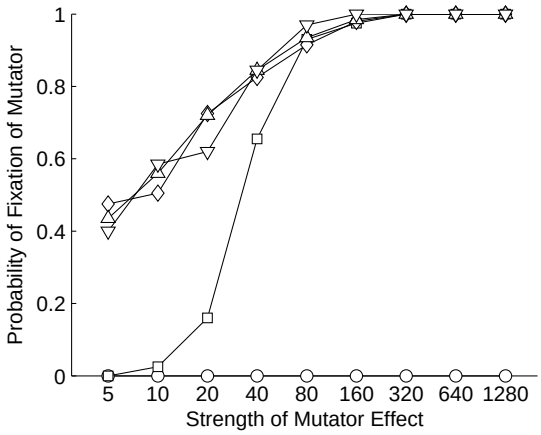

Figure 3.8: The effect of selective coefficient and strength of mutator effect on the probability of fixation of mutators (over 200 independent simulations). The strength of mutator effect m is set at log scale on x-axis. Each plot represents a different selective coefficient s: 0.01 (circle), 0.03 (square), 0.05 (diamond), 0.09 (upward-triangle), 0.15 (downward-triangle). Other parameters used in the simulation: $N = 1 \times 10^8, m = 100$

Figure 3.8 shows the effect of selective coefficient s and strength of mutator effect m on the probability of mutator fixation. The population size is fixed at 1×10^8, which is the estimated number of the actual population size in each growth well for competition experiments in Section 3.1.2 ($10^9\,\mathrm{mL}^{-1} \times 10^{-1}\,\mathrm{mL} \sim 10^8$).

When the selective coefficient is small $s = 0.01$, the fitness advantage of acquiring this beneficial mutation does not have any impact on helping mutator cells become fixed, even for mutator cells with more than 1000-fold mutation rate increase. Mutator and wild-type cells co-exist without either of them arriving at fixation. As the value of selective coefficient increases, the probability of mutator fixation also increases, and the strength of mutator effect m becomes the limiting factor ($s = 0.05, 0.09, 0.15$ points almost overlap

each other in Figure 3.8). The strength of mutator effect m here limits the upper limit of the probability of mutator fixation. For a specific value of m, as s increases, the probability of mutator fixation also increases, but cannot go above this upper limit value.

3.4 Discussion

This chapter presented an excellent example of utilizing the novel qPCR assay developed in Chapter 2 to investigate the role of spontaneous mutation on how mutator phenotype with elevated mutation rate compete with wild-type for fixation. By introducing non-lethal concentration of streptomycin as selective pressure, the competition outcomes turned from co-existence of wild-type and mutators to mutators driving wild-type to extinction as a result of mutators acquiring beneficial mutations faster through elevated mutation rate. Beneficial mutations are far rarer comparing to mutations with negative or negligible fitness effects, therefore are studied with difficulty. The experiment setup with the choice of mutators and choosing streptomycin as antibiotic selection helped the observation of beneficial mutation effect in reasonably short time span.

The concentration of streptomycin 2 $\mu g\,mL^{-1}$ was chosen to be on the lower spectrum of minimal inhibitory concentration (MIC) for *E. coli* (2–4 $\mu g\,mL^{-1}$)[127] to insure the concentration is low enough that both wild-type and mutators can grow without acquiring any beneficial mutation but also high enough to pose growth pressure that both phenotypes show decreased growth rate. A study investigated more than 900 *E. coli* isolates from meat and meat products with streptomycin MICs vary from 2 $\mu g\,mL^{-1}$ to more than 256 $\mu g\,mL^{-1}$ depending on the genetic background, and showed about 86 % strains with a low streptomycin MIC of $\leq 8\ \mu g\,mL^{-1}$ [128]. Therefore low streptomycin concentration also makes cells to acquire streptomycin resistance more easily.

By growing wild-type and mutator cells separately in media with and without added streptomycin, I estimated selective coefficients $s_{T,WR,W} = 0.08$) (Equation (3.11)) and $s_{T,MR,M} = 0.09$ (Equation (3.12))

of the streptomycin resistant mutants compared to non-resistant phenotype. By competing wild-type and mutator cells together, I estimated that under streptomycin selective pressure, mutator cells comparing to wild-type eventually exhibited a selective coefficient about $s_{\text{T,Resistant,Non-resistant}}$ $\sim$0.15 to 0.20 (Figure 3.5 third column)). The estimated values are smaller from competitive growth than those from separate growth. This discrepancy between these two sets of values comes from two sources.

First, the subscripts clearly show these selection coefficients cannot be compared directly. In order to compare them, two assumptions have to be justified. First, when grown separately, wild-type and mutator cells are indistinguishable in terms of growth rates in media both with and without antibiotics ($r_{\text{W}} = r_{\text{M}}, r_{\text{WR}} = r_{\text{MR}}$), which leads to $s_{\text{T,WR,W}} = s_{\text{T,MR,M}} = s_{\text{T,Resistant,Non-resistant}}$. This assumption is true to a great extent as the growth rates of wild-type and mutators are alike (Table 3.2) and numerically the two estimated selective coefficient values are very close 0.08 $\sim$ 0.09. The second assumption concerns the competition experiment. The selective coefficient is calculated between resistant and non-resistant phenotype. However, both resistant and non-resistant phenotype are a mixture of mutator and wild-type phenotypes. But as the competition progress, most resistant phenotype arise from mutators and most mutators become resistant, whereas most wild-type stay non-resistant phenotype. Under this assumption, the resistant phenotype only corresponds to resistant mutators, and the non-resistant phenotype only corresponds to non-resistant wild-type. The selective coefficient becomes $s_{\text{T,Resistant,Non-resistant}} = s_{\text{T,MR,W}}$. This assumption matches the simulation result as shown in Section 3.3.2.

Second, the estimated selective coefficient from separate growth experiments are calculated according to Equation (3.10) using the intrinsic growth rates of the two phenotypes when grown in isolation. This is equivalent to say that using Equation (3.10) to calculate selection coefficient assumes the nature of selection is frequency-independent. Frequency-independent selection here means there are no interactions between these two genotypes that are competing when grown together. However, from the competition experiment without streptomycin condition, we can see this assumption is not satisfied. Figure 3.4 first column shows without added selective pressure, different starting ratios will result in different competition

results. This starting ratio dependency implies there are interactions between wild-type and mutator phenotypes when grown together. It also further indicates the selective coefficient estimated value from competition experiments is the combination of fitness advantage of resistance mutation and wild-type/mutator interactions. The extracted selective coefficient values 0.15 to 0.20 are from experiments with starting mutator frequency less than equilibrium mutator frequency, and in this case, these values overestimated the true selective coefficient due to resistant mutation by including the other part of contribution from interactions between wild-type and mutators. Therefore, the actual selective coefficient due to beneficial resistance mutation from competition experiments should be less than 0.15.

It may seem surprising that mutator cells can reach fixation in such a short period of time under streptomycin selective pressure. Previous experimental work has also shown that mutators have 500-fold increase under selection of rifampin resistance [71]. To understand these results, one has to remember that the nature of adaption is organisms move toward the phenotype that best fits the current environment [129]. When adaptation is reached, no matter what the shape of the distribution of fitness is, the organism should reside at the right tail, and any beneficial mutation has to draw from the even more extreme values of that tail [130, 131]. Therefore, mutators do not have advantage if the competition happens in an environment in which wild-type is already adapted, simply because the possible beneficial mutations are limited by the fitness distribution right tail. However, for a novel environment in which neither wild-type or mutators are adapted, they no longer reside at the right tail of fitness distribution, and mutators' elevated mutation rate enables them to sample the beneficial mutations with higher probability compared to wild-type. Introducing antibiotic selective pressure is essentially shifting both wild-type and mutators away from the right tail of fitness distribution, and opens up the beneficial mutation spectrum by means of antibiotic resistance mutations.

One can also look at this from a simple mathematical model: a population of mixtures of mutators and wild-type is going through lethal antibiotic selection. Before selection, the frequencies of mutator and wild-type cells are p and $1 - p$ respectively. If the beneficial antibiotic resistance mutation rates are u for wild-

type and mu for mutators, where m is the mutation rate fold increase due to mutator phenotype (strength of mutator effect). For lethal antibiotic selection, only antibiotic resistance mutant phenotype can survive. Therefore after selection, the wild-type frequency is $(1-p)u$, and mutator frequency is pmu. After normalizing, the mutator frequency after selection p' becomes

$$\begin{aligned} p' &= \frac{pmu}{(1-p)u + pmu} \\ &= \frac{pm}{1-p+pm} \end{aligned} \tag{3.19}$$

The mutation rate u canceled out, and the mutator frequency after lethal antibiotic selection only depends on the mutator frequency before selection p and strength of mutator effect m. Figure 3.9 plots Equation (3.19) for different values of strength of mutator effect m. If mutator has no effect on mutation rate ($m = 1$), the mutator frequency does not change after selection. As mutator effect m increases, the mutator frequency after selection also increases for the same starting mutator frequency. For natural population, mutator frequency is very low, the absolute increase may seem small. But if mutator constitutes 10 % of the population, then after selection the mutator can increase to around 90 % for $m = 100$. By selecting for a specific mutant phenotype, the proportion of mutators can be greatly increased in that selected population as a result of mutators' elevated mutation rate.

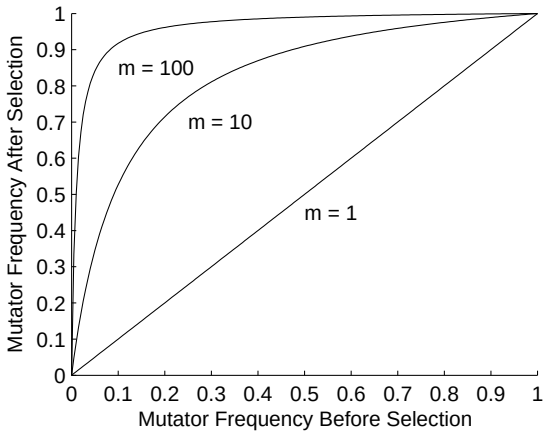

Figure 3.9: Mutator frequency increases after lethal selection. Each curve represents different mutator effect. As mutator effect increases, mutator frequency after selection also increases if starting at the same mutator frequency before selection

4

Epilogue

In 1945, Sir Alexander Fleming shared the Nobel Prize in Physiology or Medicine with Ernst Boris Chain and Sir Howard Walter Florey "for the discovery of penicillin and its curative effect in various infectious diseases" [132]. In his Nobel Lecture, Fleming gave the note of warning [133]:

> The time may come when penicillin can be bought by anyone in the shops. Then there is the danger that the ignorant man may easily underdose himself and by exposing his microbes to non-lethal quantities of the drug make them resistant. Here is a hypothetical illustration. Mr. X. has a sore throat. He buys some penicillin and gives himself, not enough to kill the

> streptococci but enough to educate them to resist penicillin. He then infects his wife. Mrs. X gets pneumonia and is treated with penicillin. As the streptococci are now resistant to penicillin the treatment fails. Mrs. X dies. Who is primarily responsible for Mrs. X's death? Why Mr. X whose negligent use of penicillin changed the nature of the microbe. *Moral*: If you use penicillin, use enough.

Fleming was right about warning the negligent use of antibiotics. Doctors around the world over-prescribe antibiotics to patients. People inappropriate use of antibiotics are still widespread. The food industry and farmers indiscriminately use low dose of antibiotics on livestock. Now Fleming's warning has become the reality: the golden age of antibiotics discovery has faded, the spread of superbugs are rising. "In essence, we are engaged in an arms race with pathogenic bacteria —– and we are losing."[134]

"The emergence of antibiotic resistance is the most eloquent example of Darwin's principle of evolution that there ever was," says David Livermore, director of the antibiotic resistance monitoring and reference laboratory of the Health Protection Agency (now part of Public Health England). "It is a war of attrition. It is naive to think we can win." [135] New antibiotic resistance is constantly generated through mutations with mutator phenotype accelerating this process. Horizontal gene transfer facilitates the spread of the newly arising resistance gene among bacteria. We have to start look beyond antibiotics, and start to explore other methods to keep bacteria at bay. Hopefully this thesis can contribute to this process by providing new methods and insight on the kinetics of evolutionary mechanisms of bacteria. We need to hurry up, because the post-antibiotic era is coming.

References

1. American Chemical Society International Historic Chemical Landmarks. Discovery and Development of Penicillin., . URL http://portal.acs.org/portal/PublicWebSite/education/whatischemistry/landmarks/flemingpenicillin/index.html.

2. Centers for Disease Control and Prevention. Antibiotic resistance threats in the United States 2013, 2013. URL http://www.cdc.gov/drugresistance/threat-report-2013/.

3. Peter J Christie and Joseph P Vogel. Bacterial type IV secretion: conjugation systems adapted to deliver effector molecules to host cells. *Trends Microbiol.*, 8(8):354–60, August 2000.

4. Steffen Backert and Thomas F Meyer. Type IV secretion systems and their effectors in bacterial pathogenesis. *Current opinion in microbiology*, 9(2):207–17, April 2006.

5. M Teuber. Spread of antibiotic resistance with food-borne pathogens. *Cell Mol Life Sci*, 56:755–63, November 1999.

6. Gary L French. The continuing crisis in antibiotic resistance. *International Journal of Antimicrobial Agents*, 36 Suppl 3:S3–7, November 2010.

7. H Allen Orr. Fitness and its role in evolutionary genetics. *Nature reviews. Genetics*, 10(8):531–9, August 2009.

8. Angus Buckling, R Craig Maclean, Michael A Brockhurst, and Nick Colegrave. The Beagle in a bottle. *Nature*, 457(7231):824–829, February 2009.

9. Santiago F Elena and Richard E Lenski. Evolution experiments with microorganisms: the dynamics and genetic bases of adaptation. *Nature reviews. Genetics*, 4(6):457–69, June 2003.

10. Jacques Monod. The Growth of Bacterial Cultures. *Annu. Rev. Microbiol.*, 3(1):371–394, October 1949.

11. Aaron Novick and Leo Szilard. Description of the chemostat. *Science*, 112(2920):715–6, December 1950.

12. Jeffrey E Barrick, Dong Su Yu, Sung Ho Yoon, Haeyoung Jeong, Tae Kwang Oh, Dominique Schneider, Richard E Lenski, and Jihyun F Kim. Genome evolution and adaptation in a long-term experiment with Escherichia coli. *Nature*, 461(7268):1243–1247, October 2009.

13. Frederick Griffith. The Significance of Pneumococcal Types. *J Hyg (Lond)*, 27(2):113–159, January 1928.

14. Oswald Avery, Colin M Macleod, and Maclyn McCarty. Studies on the chemical nature of the substance inducing transformation of pneumococcal types: induction of transformation by a desoxyribonucleic acid fraction isolated from pneumococcus Type III. *Journal of Experimental Medicine*, 79 (2):137–158, February 1944.

15. Joshua Lederberg and E L Tatum. Gene recombination in Escherichia coli. *Nature*, 158(4016):558, October 1946.

16. Frances R Slater, Mark J Bailey, Adrian J Tett, and Sarah L Turner. Progress towards understanding the fate of plasmids in bacterial communities. *FEMS microbiology ecology*, 66(1):3–13, October 2008.

17. Søren J Sørensen, Mark Bailey, Lars H Hansen, Niels Kroer, and Stefan Wuertz. Studying plasmid horizontal transfer in situ: a critical review. *Nat. Rev. Microbiol.*, 3(9), September 2005.

18. North D Zinder and Joshua Lederberg. Genetic exchange in Salmonella. *J. Bacteriol.*, 64(5):679–699, November 1952.

19. J Peter Gogarten and Jeffrey P Townsend. Horizontal gene transfer, genome innovation and evolution. *Nat. Rev. Microbiol.*, 3(9):679–87, September 2005.

20. Tal Dagan and William Martin. Ancestral genome sizes specify the minimum rate of lateral gene transfer during prokaryote evolution. *Proc. Natl. Acad. Sci. U.S.A.*, 104(3):870–5, January 2007.

21. Ravi Jain, Maria C Rivera, Jonathan E Moore, and James A Lake. Horizontal gene transfer accelerates genome innovation and evolution. *Mol. Biol. Evol.*, 20(10):1598–602, October 2003.

22. Howard Ochman, Jeffrey G Lawrence, and Eduardo A Groisman. Lateral gene transfer and the nature of bacterial innovation. *Nature*, 405(6784):299–304, May 2000.

23. Hema Prasad Narra and Howard Ochman. Of what use is sex to bacteria? *Curr. Biol.*, 16(17):R705–10, September 2006.

24. Laura S Frost, Raphael Leplae, Anne O Summers, and Ariane Toussaint. Mobile genetic elements: the agents of open source evolution. *Nat. Rev. Microbiol.*, 3(9):722–32, September 2005.

25. Hervé Tettelin, David Riley, Ciro Cattuto, and Duccio Medini. Comparative genomics: the bacterial pan-genome. *Current opinion in microbiology*, 11(5):472–7, October 2008.

26. Gary M Dunny, Byron L Brown, and Don B Clewell. Induced cell aggregation and mating in Streptococcus faecalis: evidence for a bacterial sex pheromone. *Proc. Natl. Acad. Sci. U.S.A.*, 75(7):3479–83, July 1978.

27. Don B Clewell. Conjugation in gram positive bacteria. In G Phillips and B E Funnell, editors, *Plasmid Biology*, pages 227–258. ASM Press, Washington, D.C., January 2004.

28. Jan Dirk van Elsas and Mark J Bailey. The ecology of transfer of mobile genetic elements. *FEMS microbiology ecology*, 42(2):187–97, November 2002.

29. Joshua Lederberg, Luigi L Cavalli, and Esther M Lederberg. Sex Compatibility in Escherichia Coli. *Genetics*, 37(6):720–30, November 1952.

30. Gloria del Solar, Rafael Giraldo, María J Ruiz-Echevarría, Manuel Espinosa, and Ramón Díaz-Orejas. Replication and control of circular bacterial plasmids. *Microbiology and molecular biology reviews : MMBR*, 62(2):434–64, June 1998.

31. Richard P Novick, Royston C Clowes, Stanley N Cohen, Roy Curtiss, III, Naomi Datta, and Stanley Falkow. Uniform nomenclature for bacterial plasmids: a proposal. *Bacteriological reviews*, 40(1): 168–89, March 1976.

32. Anders Norman, Lars H Hansen, and Søren J Sørensen. Conjugative plasmids: vessels of the communal gene pool. *Philos. Trans. R. Soc. Lond., B, Biol. Sci.*, 364(1527):2275–89, August 2009.

33. Abigail A Salyers, Nadja B Shoemaker, Ann M Stevens, and Lhing-Yew Li. Conjugative transposons: an unusual and diverse set of integrated gene transfer elements. *Microbiological reviews*, 59(4):579–90, December 1995.

34. Catherine A Lee and Alan D Grossman. Identification of the origin of transfer (oriT) and DNA relaxase required for conjugation of the integrative and conjugative element ICEBs1 of Bacillus subtilis. *J. Bacteriol.*, 189(20):7254–7261, October 2007.

35. Angus Buckling, Michael A Brockhurst, Michael Travisano, and Paul B Rainey. Experimental adaptation to high and low quality environments under different scales of temporal variation. *J. Evol. Biol.*, 20:296–300, January 2007.

36. Bernhard Haubold, Michael Travisano, Paul B Rainey, and Richard R Hudson. Detecting linkage disequilibrium in bacterial populations. *Genetics*, 150(4):1341–8, December 1998.

37. Trevor D Lawley, Matthew W Gilmour, James E Gunton, Leah J Standeven, and Diane E Taylor. Functional and mutational analysis of conjugative transfer region 1 (Tra1) from the IncHI1 plasmid R27. *J. Bacteriol.*, 184(8):2173–80, April 2002.

38. Andrew J Spiers, Sophie G Kahn, John Bohannon, Michael Travisano, and Paul B Rainey. Adaptive divergence in experimental populations of Pseudomonas fluorescens. I. Genetic and phenotypic bases of wrinkly spreader fitness. *Genetics*, 161(1):33–46, May 2002.

39. Cristina Alvarez-Martinez and Peter Christie. Biological diversity of prokaryotic type IV secretion systems. *Microbiology and molecular biology reviews : MMBR*, 73(4):775–808, December 2009.

40. Eric Cascales and Peter J Christie. The versatile bacterial type IV secretion systems. *Nat. Rev. Microbiol.*, 1(2):137–49, November 2003.

41. Karin Wallden, Angel Rivera-Calzada, and Gabriel Waksman. Type IV secretion systems: versatility and diversity in function. *Cell. Microbiol.*, 12(9):1203–12, September 2010.

42. L S Chavers, S A Moser, W H Benjamin, S E Banks, J R Steinhauer, A M Smith, C N Johnson, E Funkhouser, L P Chavers, A M Stamm, and K B Waites. Vancomycin-resistant enterococci: 15 years and counting. *The Journal of hospital infection*, 53(3):159–71, March 2003.

43. Elisabeth Grohmann, Günther Muth, and Manuel Espinosa. Conjugative plasmid transfer in gram-positive bacteria. *Microbiology and molecular biology reviews : MMBR*, 67(2):277–301, table of contents, June 2003.

44. Lars Andrup, Ole Jørgensen, Andrea Wilcks, Lasse Smidt, and Gert B Jensen. Mobilization of "nonmobilizable" plasmids by the aggregation-mediated conjugation system of Bacillus thuringiensis. *Plasmid*, 36(2):75–85, September 1996.

45. Bruce R Levin and Carl T Bergstrom. Bacteria are different: observations, interpretations, speculations, and opinions about the mechanisms of adaptive evolution in prokaryotes. *Proc. Natl. Acad. Sci. U.S.A.*, 97(13):6981–5, June 2000.

46. Salvado E Luria and Max Delbrück. Mutations of Bacteria from Virus Sensitivity to Virus Resistance. *Genetics*, 28(6):491–511, November 1943.

47. Michael M Mwangi, Shang Wei Wu, Yanjiao Zhou, Krzysztof Sieradzki, Herminia de Lencastre, Paul Richardson, David Bruce, Edward Rubin, Eugene Myers, Eric D Siggia, and Alexander Tomasz. Tracking the in vivo evolution of multidrug resistance in Staphylococcus aureus by whole-genome sequencing. *Proc. Natl. Acad. Sci. U.S.A.*, 104(22):9451–6, May 2007.

48. Michael Lynch. Evolution of the mutation rate. *Trends in genetics : TIG*, 26(8):345–52, August 2010.

49. John Drake, Brian Charlesworth, Deborah Charlesworth, and James F Crow. Rates of spontaneous mutation. *Genetics*, 148(4), April 1998.

50. Jeffrey H Miller. Spontaneous mutators in bacteria: insights into pathways of mutagenesis and repair. *Annual review of microbiology*, 50:625–43, January 1996.

51. Jens-Peter Horst, Te-hui Wu, and Martin G Marinus. Escherichia coli mutator genes. *Trends Microbiol.*, 7(1):29–36, January 1999.

52. J Eugene LeClerc, Baoguang Li, William L Payne, and Thomas A Cebula. High mutation frequencies among Escherichia coli and Salmonella pathogens. *Science*, 274(5290):1–4, November 1996.

53. Antonio Oliver, Fernando Baquero, and Jesús Blázquez. The mismatch repair system (mutS, mutL and uvrD genes) in Pseudomonas aeruginosa: molecular characterization of naturally occurring mutants. *Mol. Microbiol.*, 43(6):1641–50, March 2002.

54. Pauline Funchain, Annie Yeung, Jean L Stewart, Rose Lin, Malgorzata M Slupska, and Jeffrey H Miller. The consequences of growth of a mutator strain of Escherichia coli as measured by loss of function among multiple gene targets and loss of fitness. *Genetics*, 154(3):1–12, March 2000.

55. F Taddei, M Radman, J Maynard-Smith, B Toupance, P H Gouyon, and B Godelle. Role of mutator alleles in adaptive evolution. *Nature*, 387(6634):700–2, June 1997.

56. Olivier Tenaillon, Bruno Toupance, Hervé Le Nagard, Frrançois Taddei, and Bernard Godelle. Mutators, population size, adaptive landscape and the adaptation of asexual populations of bacteria. *Genetics*, 152(2):485–93, June 1999.

57. Olivier Tenaillon, Hervé Le Nagard, Bernard Godelle, and François Taddei. Mutators and sex in bacteria: conflict between adaptive strategies. *Proc. Natl. Acad. Sci. U.S.A.*, 97(19):10465–70, September 2000.

58. P R Painter. Mutator genes and selection for the mutation rate in bacteria. *Genetics*, 79(4):649–60, April 1975.

59. Mark A Bedau and Norman H Packard. Evolution of evolvability via adaptation of mutation rates. *Bio Systems*, 69(2-3):143–62, May 2003.

60. Kaare Jyssum. Observations on two types of genetic instability in Escherichia coli. *Acta pathologica et microbiologica Scandinavica*, 48:113–20, January 1960.

61. Michael D Gross and Eli C Siegel. Incidence of mutator strains in Escherichia coli and coliforms in nature. *Mutation research*, 91(2):107–10, March 1981.

62. Ivan Matic, Miiroslav Radman, François Taddei, Bertrand Picard, Catherine Doit, Edouard Bingen, Erick Denamur, and Jacques Elion. Highly variable mutation rates in commensal and pathogenic Escherichia coli. *Science*, 277(5333):1–3, September 1997.

63. Antonio Oliver, Rafael Cantón, Pilar Campo, Fernando Baquero, and Jesús Blázquez. High frequency of hypermutable Pseudomonas aeruginosa in cystic fibrosis lung infection. *Science*, 288(5469):1251–4, May 2000.

64. Lucinda M Hall and Stephanie K Henderson-Begg. Hypermutable bacteria isolated from humans–a critical analysis. *Microbiology (Reading, England)*, 152(Pt 9):2505–14, September 2006.

65. Federico Román, Rafael Cantón, María Pérez-Vázquez, Fernando Baquero, and José Campos. Dynamics of long-term colonization of respiratory tract by Haemophilus influenzae in cystic fibrosis patients shows a marked increase in hypermutable strains. *Journal of clinical microbiology*, 42(4):1450–9, April 2004.

66. Anne-Laure Prunier, Brigitte Malbruny, Muriel Laurans, Jacques Brouard, Jean-François Duhamel, and Roland Leclercq. High rate of macrolide resistance in Staphylococcus aureus strains from patients with cystic fibrosis reveals high proportions of hypermutable strains. *The Journal of infectious diseases*, 187(11):1709–16, June 2003.

67. Jeffrey H Miller. The relevance of bacterial mutators to understanding human cancer. *Cancer surveys*, 28:141–53, January 1996.

68. Guillaume Lambert, Luis Estévez-Salmeron, Steve Oh, David Liao, Beverly M Emerson, Thea D Tlsty, and Robert H Austin. An analogy between the evolution of drug resistance in bacterial communities and malignant tissues. *Nature reviews. Cancer*, 11(5):375–82, May 2011.

69. Christopher F Gentile, Szi-Chieh Yu, Sebastian Akle Serrano, Philip J Gerrish, and Paul D Sniegowski. Competition between high- and higher-mutating strains of Escherichia coli. *Biology Letters*, 7(3): 422–4, June 2011.

70. W Tröbner and R Piechocki. Competition between isogenic mutS and mut+ populations of Escherichia coli K12 in continuously growing cultures. *Molecular & general genetics : MGG*, 198(1): 175–6, January 1984.

71. Emily F Mao, Laura Lane, Jean Lee, and Jeffrey H Miller. Proliferation of mutators in A cell population. *J Bacteriol*, 179(2):1–7, January 1997.

72. Mark M Tanaka, Carl T Bergstrom, and Bruce R Levin. The evolution of mutator genes in bacterial populations: the roles of environmental change and timing. *Genetics*, 164(3):1–12, July 2003.

73. J M Travis and E R Travis. Mutator dynamics in fluctuating environments. *Proc. Biol. Sci.*, 269(1491): 591–7, March 2002.

74. Lars Andrup and Katja Andersen. A comparison of the kinetics of plasmid transfer in the conjugation systems encoded by the F plasmid from Escherichia coli and plasmid pCF10 from Enterococcus faecalis. *Microbiology*, 145(8):2001–2009, August 1999.

75. Randal E Fox, Xue Zhong, Stephen M Krone, and Eva M Top. Spatial structure and nutrients promote invasion of IncP-1 plasmids in bacterial populations. *ISME J*, 2(10):1024–1039, June 2008.

76. R Gregory, J R Saunders, and V A Saunders. Rule-based modelling of conjugative plasmid transfer and incompatibility. *Biosystems*, 91(1):201–215, January 2008.

77. Stephen M Krone, Ruinan Lu, Randal Fox, Haruo Suzuki, and Eva M Top. Modelling the spatial dynamics of plasmid transfer and persistence. *Microbiology (Reading, England)*, 153(Pt 8):2803–16, August 2007.

78. Loukia N Lili, Nicholas F Britton, and Edward J Feil. The Persistence of Parasitic Plasmids. *Genetics*, 177(1):399–405, July 2007.

79. José M Ponciano, Leen De Gelder, Eva M Top, and Paul Joyce. The Population Biology of Bacterial Plasmids: A Hidden Markov Model Approach. *Genetics*, 176(2):957–968, December 2006.

80. Allan R Willms, Paul D Roughan, and Jack A Heinemann. Static recipient cells as reservoirs of antibiotic resistance during antibiotic therapy. *Theor Popul Biol*, 70:436–51, December 2006.

81. Xue Zhong, JarosŁaw E l, Eva M Top, and Stephen M Krone. Accounting for mating pair formation in plasmid population dynamics. *J. Theor. Biol.*, 262(4):711–719, February 2010.

82. Bjarke B Christensen, Claus Sternberg, and Soren Molin. Bacterial plasmid conjugation on semi-solid surfaces monitored with the green fluorescent protein (GFP) from Aequorea victoria as a marker. *Gene*, 173(1 Spec No):59–65, 1996.

83. Bo Normander, Bjarke B Christensen, Soren Molin, and Niels Kroer. Effect of Bacterial Distribution and Activity on Conjugal Gene Transfer on the Phylloplane of the Bush Bean (Phaseolus vulgaris). *Applied and Environmental Microbiology*, 64(5):1902–9, May 1998.

84. Margaret Clarke, Lucinda Maddera, Robin L Harris, and Philip M Silverman. F-pili dynamics by live-cell imaging. *Proc. Natl. Acad. Sci. U.S.A.*, 105(46):17978–81, November 2008.

85. Mark Achtman. Mating aggregates in Escherichia coli conjugation. *J. Bacteriol.*, 123(2):505–15, August 1975.

86. Marjorie Russel, Nora A Linderoth, and Andrej Šali. Filamentous phage assembly: variation on a protein export theme. *Gene*, 192(1):23–32, June 1997.

87. Yukinori Hirota. The effect of acridine dyes on mating type factors in Escherichia coli. *Proc. Natl. Acad. Sci. U.S.A.*, 46:57–64, January 1960.

88. Zhenmao Wan, Joseph Varshavsky, Sushma Teegala, Jamille McLawrence, and Noel L Goddard. Measuring the Rate of Conjugal Plasmid Transfer in a Bacterial Population Using Quantitative PCR. *Biophysical Journal*, 101(1):237–244, 2011.

89. Haukur Gudnason, Martin Dufva, D D Bang, and Anders Wolff. Comparison of multiple DNA dyes for real-time PCR: effects of dye concentration and sequence composition on DNA amplification and melting temperature. *Nucleic Acids Research*, 35(19):e127–e127, October 2007.

90. Carl T Bergstrom, Marc Lipsitch, and Bruce R Levin. Natural selection, infectious transfer and the existence conditions for bacterial plasmids. *Genetics*, 155:1505–19, August 2000.

91. Bruce R Levin and Frank M Stewart. The Population Biology of Bacterial Plasmids: A PRIORI Conditions for the Existence of Mobilizable Nonconjugative Factors. *Genetics*, 94(2):425–43, February 1980.

92. Peter D Lundquist and Bruce R Levin. Transitory Derepression and the Maintenance of Conjugative Plasmids . *Genetics*, 113(3):483–97, July 1986.

93. Frank M Stewart and Bruce R Levin. The Population Biology of Bacterial Plasmids: A PRIORI Conditions for the Existence of Conjugationally Transmitted Factors. *Genetics*, 87(2):209–228, October 1977.

94. Jacques Monod. Recherches sur la Croissance des Cultures Bacteriennes. January 1942.

95. Alan Kingsman and Neil Willetts. The requirements for conjugal DNA synthesis in the donor strain during flac transfer. *J Mol Biol*, 122:287–300, July 1978.

96. Guennadi Sezonov, Danièle Joseleau-Petit, and Richard D'Ari. Escherichia coli Physiology in Luria-Bertani Broth. *J. Bacteriol.*, 189(23):8746–8749, November 2007.

97. John Cullum, J F Collins, and Paul Broda. Factors affecting the kinetics of progeny formation with F'lac in Escherichia coli K12. *Plasmid*, 1:536–44, September 1978.

98. Emory L Ellis and Max Delbrück. THE GROWTH OF BACTERIOPHAGE. *The Journal of General Physiology*, 22(3):365–84, January 1939.

99. Abraham Lin, Jose Jimenez, Julien Derr, Pedro Vera, Michael L Manapat, Kevin M Esvelt, Laura Villanueva, David R Liu, and Irene A Chen. Inhibition of Bacterial Conjugation by Phage M13 and Its Protein g3p: Quantitative Analysis and Model. *PLOS ONE*, 6(5):e19991, May 2011.

100. L Simonsen, D M Gordon, F M Stewart, and B R Levin. Estimating the rate of plasmid transfer: an end-point method. 136:2319–25, November 1990.

101. David M Gordon. Rate of plasmid transfer among Escherichia coli strains isolated from natural populations. 138:17–21, January 1992.

102. Tine R Licht, Bjarke B Christensen, Karen A Krogfelt, and Soren Molin. Plasmid transfer in the animal intestine and other dynamic bacterial populations: the role of community structure and environment. *Microbiology*, January 1999.

103. David B. Dusenbery. *Living at Micro Scale*. Harvard University Press, 2008.

104. Marianne de De Paepe, Marianne de Paepe, Silvia de Monte, Lydia Robert, Silvia de De Monte, Ariel B. Lindner, and François Taddei. Emergence of Variability in Isogenic Escherichia coli Populations Infected by a Filamentous Virus. *PLOS ONE*, 5(7):e11823, July 2010.

105. D A Marvin and Barbara Hohn. Filamentous bacterial viruses. *Bacteriological Reviews*, 33(2):172–209, June 1969.

106. William O Salivar, Helen Tzagoloff, and David Pratt. Some Physical-Chemical and Biological Properties of the Rod-Shaped Coliphage M13. *Virology*, 24:359–71, November 1964.

107. Paul D Sniegowski, Philip J Gerrish, and Richard E Lenski. Evolution of high mutation rates in experimental populations of E. coli. *Nature*, 387(6634):703–5, June 1997.

108. Aaron C Shaver, Peter G Dombrowski, Joseph Y Sweeney, Tania Treis, Renata M Zappala, and Paul D Sniegowski. Fitness evolution and the rise of mutator alleles in experimental Escherichia coli populations. *Genetics*, 162(2):557–66, October 2002.

109. Erick Denamur, Stéphane Bonacorsi, Antoine Giraud, Patrick Duriez, Farida Hilali, Christine Amorin, Edouard Bingen, Antoine Andremont, Bertrand Picard, François Taddei, Ivan Matic, E. Denamur, S. Bonacorsi, A. Giraud, P. Duriez, F. Hilali, C. Amorin, E. Bingen, A. Andremont, B. Picard, F. Taddei, and I. Matic. High Frequency of Mutator Strains among Human Uropathogenic Escherichia coli Isolates. *Journal of Bacteriology*, 184(2):605–609, January 2002.

110. Baoguang Li, Ho-Ching T Tsui, J Eugene LeClerc, Manashi Dey, Malcolm E Winkler, and Thomas A Cebula. Molecular analysis of mutS expression and mutation in natural isolates of pathogenic Escherichia coli. *Microbiology (Reading, England)*, 149(Pt 5):1323–1331, May 2003.

111. Thomas A Kunkel and Dorothy A Erie. DNA MISMATCH REPAIR*. *Annu. Rev. Biochem.*, 74(1): 681–710, June 2005.

112. Guo-Min Li. Mechanisms and functions of DNA mismatch repair. *Cell Res.*, 18(1):85–98, January 2008.

113. A Oliver and A Mena. Bacterial hypermutation in cystic fibrosis, not only for antibiotic resistance. *Clinical microbiology and infection : the official publication of the European Society of Clinical Microbiology and Infectious Diseases*, 16(7), July 2010.

114. Paul Modrich and Robert Lahue. Mismatch repair in replication fidelity, genetic recombination, and cancer biology. *Annual review of biochemistry*, pages 1–33, January 1996.

115. Changill Ban, Murray Junop, and Wei Yang. Transformation of MutL by ATP binding and hydrolysis: a switch in DNA mismatch repair. *Cell*, January 1999.

116. Fang Chen, Wei-Qiao Liu, Zhen-Hong Liu, Qing-Hua Zou, Ye Wang, Yong-Guo Li, Jin Zhou, Abraham Eisenstark, Randal Johnston, Gui-Rong Liu, Bao-Feng Yang, and Shu-Lin Liu. mutL as a genetic switch of bacterial mutability: turned on or off through repeat copy number changes. *FEMS Microbiology Letters*, 312(2):126–132, November 2010.

117. H. Lee, E. Popodi, H. Tang, and P. L. Foster. PNAS Plus: Rate and molecular spectrum of spontaneous mutations in the bacterium Escherichia coli as determined by whole-genome sequencing. *Proceedings of the National Academy of Sciences*, 109(41):E2774–E2783, October 2012.

118. JC Galán, MC Turrientes, and MR Baquero. Mutation rate is reduced by increased dosage of mutL gene in Escherichia coli K-12. *FEMS Microbiology*, January 2007.

119. Andrew P. Carter, William M. Clemons, Ditlev E. Brodersen, Robert J. Morgan-Warren, Brian T. Wimberly, and V. Ramakrishnan. Functional insights from the structure of the 30S ribosomal subunit and its interactions with antibiotics. *Nature*, 407(6802):340–348, September 2000.

120. T Ruusala and C G Kurland. Streptomycin preferentially perturbs ribosomal proofreading. *Molecular and General Genetics MGG*, January 1984.

121. Li Ren, Sayeedur M Rahman, and Zafri M Humayun. Escherichia coli Cells Exposed to Streptomycin Display a Mutator Phenotype. *Journal of Bacteriology*, 181(3):1043–1044, February 1999.

122. Lars Boe. Translational errors as the cause of mutations in Escherichia coli. *Molecular and General Genetics MGG*, 231(3):469–471, January 1992.

123. Tomoya Baba, Takeshi Ara, Miki Hasegawa, Yuki Takai, Yoshiko Okumura, Miki Baba, Kirill A Datsenko, Masaru Tomita, Barry L Wanner, and Hirotada Mori. Construction of Escherichia coli K-12 in-frame, single-gene knockout mutants: the Keio collection. *Molecular Systems Biology*, 2, February 2006.

124. EZ Rich Defined Medium, . URL http://www.genome.wisc.edu/resources/protocols/ezmedium.htm.

125. Ronald A Fisher. *The Genetical Theory of Natural Selection*. A Complete Variorum Edititon. Oxford University Press, October 1999.

126. Luis-Miguel Chevin. On measuring selection in experimental evolution. *Biology Letters*, 7(2):210–213, April 2011.

127. William Martindale. *Martindale: The Extra Pharmacopoeia*. Pharmaceutical Press, London, UK, 28th edition, 1982.

128. Marianne Sunde and Madelaine Norström. The genetic background for streptomycin resistance in Escherichia coli influences the distribution of MICs. *J. Antimicrob. Chemother.*, 56(1):87–90, July 2005.

129. H Allen Orr. The genetic theory of adaptation: a brief history. *Nature Reviews Genetics*, 2005.

130. John H Gillespie. A simple stochastic gene substitution model. *Theoretical Population Biology*, 23(2): 202–215, April 1983.

131. John H Gillespie. Molecular evolution over the mutational landscape. *Evolution*, 38(5):1116–1129, September 1984.

132. The Nobel Prize in Physiology or Medicine 1945. URL http://www.nobelprize.org/nobel_prizes/medicine/laureates/1945/.

133. Alexander Fleming. Sir Alexander Fleming - Nobel Lecture: Penicillin. URL http://www.nobelprize.org/nobel_prizes/medicine/laureates/1945/fleming-lecture.html.

134. The antibiotic alarm. *Nature*, 495(141), March 2013.

135. Sarah Boseley. Are you ready for a world without antibiotics? *The Guardian*, August 2010.